SCHOOL OF ADVANCED STUDIES OF THE ROMANIAN ACADEMY DOCTORAL SCHOOL OF CHEMICAL SCIENCES PETRU PONI INSTITUTE OF MACROMOLECULAR CHEMISTRY CHEMISTRY Field

MICRO AND NANOSTRUCTURED BIOMATERIALS BASED ON POLYSACCHARIDES: PREPARATION, STRUCTURE, AND PROPERTIES SUMMARY OF THE DOCTORAL THESIS

Ph.D. supervisor:
Dr. Habil. MARCELA MIHAI

Ph.D. student: ELENA-DANIELA LOTOS

ROMANIAN ACADEMY

Petru Poni Institute of Macromolecular Chemistry

Mrs	/Ms						
14110./	TATO	 · • • • • • • • • • • • • • • • • • • •	 	 	 	 	

We would like to inform you that on 15.12.2025, at 11⁰⁰, in the Conference Room of the "Acad. Bogdan C. Simionescu" Pavilion at the Petru Poni Institute of Macromolecular Chemistry in Iasi, the public defense of the doctoral thesis "Micro- and nanostructured biomaterials based on polysaccharides: preparation, structure, and properties", authored by bioengineer Elena-Daniela LOTOS, in order to obtain the scientific title of doctor.

PRESIDENT: CS I Dr. Maria CAZACU

Petru Poni Institute of Macromolecular Chemistry, Iasi

DOCTORAL SUPERVISOR: CS I Dr. habil. Marcela MIHAI

Petru Poni Institute of Macromolecular Chemistry, Iasi

REFEREES: CS I Dr. Habil. Luminița MARIN

Petru Poni Institute of Macromolecular Chemistry, Iasi

Conf. Dr. Robert-Vasile GRADINARU

Alexandru Ioan Cuza University, Iasi

Conf. Dr. Ing. Florin CIOLACU

Gheorghe Asachi Technical University, Iasi

In accordance with the Regulations on the organization and conduct of doctoral studies for the awarding of scientific titles in the Romanian Academy, we are sending you the summary of the doctoral thesis and kindly request your feedback and comments. We would also like to invite you to attend the public defense of the doctoral thesis.

Director PPICM,

CS I Dr. Valeria HARABAGIU

TABLE OF CONTENTS THESIS/SUMMARY

LIST OF ABREVIATIONS	I
LIST OF FIGURES AND SCHEMES	III
LIST OF TABLESX	II
INTRODUCTION1	<u>/1</u>
PART I. CURRENT STATE OF KNOWLEDGE	6
CHAPTER 1. Micro- and nanostructured biomaterials based on polysaccharides	6
1.1. Classification and applications of biomaterials	6
1.1.1. Classification of biomaterials	6
1.1.2. Applications of biomaterials	.8
1.2. Polysaccharides	12
1.2.1. Classification of polysaccharides	12
1.2.2. Alginate	15
1.2.3. Chitosan	17
1.2.4. Chondroitin sulfate	18
1.2.5. Xanthan gum	20
1.2.6. Modification of polysaccharides	22
1.3. Polysaccharide-based materials	24
1.3.1. Polysaccharide-based polyelectrolyte complexes	24
1.3.2. Polysaccharide-based hydrogels	30
1.3.3. Polysaccharide-based emulsions.	38
1.4. Conclusions, challenges, and perspectives	47
CHAPTER 2. Experimental Part	50
2.1. Used materials	50
2.2. Synthesis of chitosan- <i>g</i> -poly(<i>N</i> -isopropylacrylamide) hybrid copolymer	52
2.3. Methods for obtaining micro- and nanostructured materials	53
2.3.1. Preparation of interpolymeric complexes based on polysaccharides and zein5	53
2.3.2. Preparation of interpolymeric complexes based on chitosan and PNIPAM	54
	nd 55

2.3.4. Preparation of composite hydrogels based on polysaccharides and CaCO ₃	56
2.3.4.1. Preparation of hydrogels with calcium alginate and CaCO ₃	56
2.3.4.2. Preparation of hydrogels with calcium alginate, polyelectrolyte comand CaCO ₃	_
2.3.5. Preparation of oil-in-water emulsions based on xanthan gum	56
2.3.6. Application of oil-in-water emulsions on textile substrates	57
2.4. Characterization methods.	57
2.4.1. Dynamic light scattering and electrophoretic light scattering	57
2.4.2. Ionic charge density determination	58
2.4.3. Reverse conductometric titrations	59
2.4.4. Scanning electron microscopy	59
2.4.5. Scanning transmission electron microscopy	60
2.4.6. Atomic force microscopy	60
2.4.7. Analysis of the size and shape of emulsion droplets	60
2.4.8. Circular dichroism	60
2.4.9. Thermogravimetric analysis	60
2.4.10. RAMAN spectroscopy	61
2.4.11. X-ray diffraction.	61
2.4.12. Nuclear magnetic resonance spectroscopy	61
2.4.13. Infrared spectroscopy	62
2.4.14. Fluorescence spectroscopy	63
2.4.15. Interfacial tension.	64
2.4.16. Conductivity, pH, and turbidity	64
2.5. Interaction of complex nanoparticles with bioactive molecules	65
2.5.1. Interaction of complex nanoparticles with ciprofloxacin	65
2.5.2. Interaction of Chit/PNIPAM complex nanoparticles with curcumin	65
2.6. Modification of surfaces with complex nanoparticles of polysaccharides/zein	66
2.7. Biocompatibility tests	66
2.7.1. Biocompatibility tests of hydrogels	66
2.7.2. Biocompatibility tests of emulsions	67

2.8. Assessment of skin hydration and comfort indices upon application of emulsions68
2.8.1. Assessment of skin hydration through the application of emulsions68
2.8.2. Analysis of comfort indices
2.9. Antibacterial activity tests
2.9.1. Testing of surfaces modified with polymer complex nanoparticles69
2.9.2. Testing of oil-in-water emulsions
PART II. ORIGINAL RESULTS71/5
CHAPTER 3. Micro- and nanostructured biomaterials based on polysaccharides, in the form of interpolymeric complexes71/5
3.1. Preparation and characterization of non-stoichiometric interpolymer complexes based on polysaccharides and other natural polymers72/5
3.1.1. Characterization of zein solutions/dispersions73/5
3.1.2. Nanoparticles of polysaccharide/zein complexes
3.1.3. Nanoparticles of zein/polysaccharide complexes79/6
3.1.4. Nanoparticles of zein, polysaccharides, and ciprofloxacin complexes85/8
3.1.5. Modification of the surface of a nonwoven material with complex nanoparticles
3.1.6. Study of the antibacterial activity of modified surfaces89/10
3.1.7. Partial conclusions90
3.2. Preparation and characterization of interpolymeric complexes based on polysaccharides and synthetic polymers91/11
3.2.1. Study of the physicochemical properties of Chit/PNIPAM complexes92/11
3.2.2. The behavior of Chit/PNIPAM complexes at different temperatures108/12
3.2.3. The effect of ionic strength on the characteristics of Chit/PNIPAM complexes
3.2.4. The ability to load bioactive molecules into Chit/PNIPAM complexes
3.2.5. Partial conclusions
CAPITOLUL 4. Micro- and nanostructured biomaterials based on grafted chitosan, in the form of polyplexes
4.1. Preparation and characterization of chitosan- <i>g</i> -poly(<i>N</i> -isopropylacrylamide) copolymer
4.1.1. Characterization of the Chit-g-PNIPAM copolymer124/17

4.1.1.1. FTIR-ATR spectroscopy
4.1.1.2. ¹ H-NMR spectroscopy
4.1.1.3. Thermogravimetric analysis
4.1.1.4. Reverse conductometric titration
4.1.2. The influence of temperature on the properties of Chit-g-PNIPAM solutions
4.1.3. Partial conclusions
4.2. Preparation and characterization of Chit-g-PNIPAM and DNA-based polyplexes
4.2.1. Physical and chemical properties of Chit-g-PNIPAM/DNA polyplexes
4.2.2. Study of the thermal response of Chit-g-PNIPAM/DNA polyplexes139/24
4.2.3. Stability of Chit-g-PNIPAM/DNA polyplexes to ionic strength variation143
4.2.4. Stability of Chit-g-PNIPAM/DNA polyplexes in biological fluids146/25
4.2.5. The DNA-binding affinity of the Chit- <i>g</i> -PNIPAM copolymer149
4.2.6. Evaluation of DNA structure in polyplexes with Chit-g-PNIPAM150
4.2.7. Conclusions
CAPITOLUL 5. Micro- and nanostructured biomaterials based on calcium alginate, in the form of composite hydrogels
5.1. Preliminary characterization of calcium alginate 151
5.2. In situ preparation and characterization of ACa-CaCO ₃ composite hydrogels
5.3. Preparation and characterization of NPEC nanoparticles
5.4. Preparation and characterization of multicomponent ACa-NPEC-CaCO ₃ hydrogels
5.5. Conclusions
CAPITOLUL 6. Micro- and nanostructured xanthan-based biomaterials, in the form of oil-in-water emulsions
6.1. Preliminary characterization of macerated oil from Daucus Carota174
6.2. Formulations optimization for oil-in-water emulsion preparation174/30
6.2.1. The influence of macerated carrot oil content on the characteristics of oil-in-water emulsions

6.2.2. Influence of surfactant content on the characteristics of oil-in-water emulsions
6.2.3. Influence of polysaccharide content on the characteristics of oil-in-water emulsions
6.3. Study of the biological properties of oil-in-water emulsions183/31
6.3.1. The cytotoxic behavior of oil-in-water emulsions183/31
6.3.2. Antimicrobial activity of oil-in-water emulsions
6.4. Assessment of skin hydration by applying oil-in-water emulsions
6.5. Preparation of textile supports treated with oil-in-water emulsions and their evaluation as cosmetic textiles
6.5.1. Analysis of comfort indices187/33
6.5.1. Analysis of comfort indices
6.5.2. Assessment of skin hydration through the application of textiles
6.5.2. Assessment of skin hydration through the application of textiles functionalized with oil-in-water emulsions
6.5.2. Assessment of skin hydration through the application of textiles functionalized with oil-in-water emulsions
6.5.2. Assessment of skin hydration through the application of textiles functionalized with oil-in-water emulsions

INTRODUCTION

General conceptual references. Importance, relevance, and motivation of the doctoral thesis

Polysaccharide-based biomaterials represent an important category of materials in the field of biomedical engineering and sustainable materials science. These natural polymers, derived from renewable sources, exhibit remarkable biocompatibility, biodegradability, and chemical versatility, making them extremely attractive for a wide range of applications in the medical, pharmaceutical, food, and environmental protection fields.

Polysaccharides such as chitosan, alginate, chondroitin sulfate, and hyaluronic acid are intrinsically biocompatible, meaning they can interact with biological systems without causing toxic or immunogenic reactions. Their biodegradable properties ensure their breakdown into non-toxic by-products through natural metabolic pathways, eliminating the need for surgical removal in many biomedical applications and reducing environmental impact.

Derived from natural sources such as plants, algae, and microorganisms, polysaccharides represent a class of sustainable, environmentally friendly materials. Their widespread availability and renewable nature support the circular economy, thereby reducing dependence on petroleum-based synthetic polymers. Polysaccharides contain reactive functional groups (hydroxyl, amino, and carboxyl) that allow for a wide range of chemical modifications and enable the development of materials with specific properties, such as bioactivity, solubility, and mechanical strength, which can be processed into a variety of forms, including hydrogels, films, fibers, and nanoparticles.

Therefore, to obtain micro- and nanostructured biomaterials, polysaccharides can be used in combination with other natural or synthetic macromolecules, with different functional groups or the ability to respond to various external or internal stimuli. The properties of the biomaterials to be obtained can be adjusted by choosing the appropriate polymers according to the intended applications.

The motivation for developing micro- and nanostructured biomaterials based on polysaccharides is supported in this context from both a theoretical and practical point of view. The micro- and nanostructuring of polysaccharides has various advantages that may be favorable for their possible applications: increased specific surface area for drug loading and controlled and targeted release of bioactive agents, sorption capacity for various

organic and inorganic pollutants, mechanical properties suitable for tissue engineering or for the formation of films and membranes. The motivation for developing micro- and nanostructured polysaccharide-based biomaterials is based on their intrinsic properties, such as non-toxicity, functional versatility, and environmental sustainability. These materials respond to current research challenges while aligning with global goals of green innovation and the circular bioeconomy.

Alignment of the topic with international, national, and research community concerns

As a result of increased interest in the development of biocompatible, biodegradable, and sustainable materials, the field of polysaccharide-based biomaterials has experienced significant growth worldwide in recent years. Chapter 1 provides an analysis of current research trends, highlighting the importance of this field through a detailed review of the literature. The literature review outlines recent advances in the design, characterization, and use of polysaccharides in various fields, such as tissue engineering, controlled drug delivery, and tissue regeneration. Also, on a national level, the study of polysaccharides and polysaccharide-based materials has increasingly started to get more attention from the scientific community in different research fields. Considering these factors, the choice of this field for the development of the doctoral thesis aims to enrich the class of micro- and nanostructured biomaterials based on polysaccharides by obtaining, characterizing, and evaluating new functional structures with optimized physicochemical and biological properties.

The topic of the doctoral thesis is related to the research interests of the *Functional Polymers Laboratory* at the *Petru Poni Institute of Macromolecular Chemistry in Iași*, the laboratory's objective being the scientific development in the field of multifunctional materials, through the synthesis and use of a wide range of synthetic and natural ionic polymers, with pre-established functional groups and architectures, obtaining complex multicomponent systems with applications in various fields.

The research team at the Functional Polymers Laboratory has previously studied polyelectrolyte complexes based on chitosan and other synthetic polyelectrolytes (Mihai, 2009; 2011), generally for use as flocculants in applications for cleaning polluted water. The innovation of the research proposed in this doctoral thesis involves obtaining microand nanostructured biomaterials based on polysaccharides, in various forms, for use in medical or cosmetic applications.

Thesis objectives and experimental methodology

Therefore, the main objective of this doctoral thesis was to obtain new micro- and nanostructured biomaterials based on polysaccharides and other natural or synthetic polymers and to characterize them in terms of their structure and properties.

From this main objective, five secondary objectives were derived:

- Preparation and characterization of non-stoichiometric interpolymeric complexes based on polysaccharides and other natural polymers;
- Preparation and characterization of interpolymeric complexes based on polysaccharides and synthetic polymers;
- Preparation and characterization of polyplexes based on Chit-g-PNIPAM and DNA;
- Preparation and characterization of micro- and nanostructured biomaterials based on calcium alginate, in the form of composite hydrogels;
- Preparation and characterization of micro- and nanostructured xanthan-based biomaterials, in the form of oil-in-water emulsions.

Content of the doctoral thesis

The doctoral thesis entitled "Micro- and nanostructured biomaterials based on polysaccharides: preparation, structure, properties" covers 196 pages and comprises six chapters, including 128 figures, 17 tables, 11 equations, one diagram, and 307 bibliographical references. The doctoral thesis is structured in two main sections: Part I, entitled "Current state of knowledge," consists of one chapter and presents a synthesis of the scientific context that motivates the choice of materials and experimental methods used, while Part II, entitled "Original Results," is structured in five chapters and presents the original results obtained in the studies carried out in this doctoral thesis.

The current state of knowledge, presented in **Chapter 1**, highlights the importance of biomaterials in the scientific field, especially polysaccharide-based biomaterials, as well as some important properties of polysaccharides that will be used in experimental studies. Also, the principal methods for obtaining micro- and nanostructured biomaterials in the form of polyelectrolyte complexes, hydrogels, or emulsions reported in the specialized literature are analyzed and detailed, as well as the main applications of these materials.

Chapter 2 presents the materials used in the doctoral thesis, including a detailed description of the experimental methods used to obtain micro- and nanostructured biomaterials based on polysaccharides. The chapter presents methods for characterizing

materials in terms of their structure and properties, as well as methods for evaluating the potential applications of the obtained biomaterials.

Chapter 3 presents the preparation of two different types of non-stoichiometric polyelectrolyte complexes: polysaccharides/other natural polymers and polysaccharides/synthetic polymers. This chapter presents detailed information on the preparation of non-stoichiometric polyelectrolyte complexes and their characterization using a variety of experimental methods. It also identifies the main elements that influence the properties of the complexes, and the most stable ones are selected for the preparation of three-component complexes using different active molecules.

Chapter 4 presents the synthesis and characterization of a copolymer obtained by grafting poly(*N*-isopropylacrylamide) polymer onto chitosan, followed by the investigation of the electrostatic interaction between the copolymer and two DNA macromolecules of different lengths. The materials obtained are characterized by appropriate methods to confirm their chemical structure and to determine the properties of interest for use in specific applications, such as gene delivery.

Chapter 5 proposes a new method for obtaining homogeneous, highly organized hydrogels using a dispersion of calcium alginate and CaCl2 solution, the latter having a dual role: as a source of divalent ions for cross-linking alginate chains and as nucleation centers for CaCO3 crystallization. In addition, the MTS test showed that cross-linked hydrogels have significant cell viability even after 48 hours. The study also demonstrates the feasibility of the method in more complex systems by adding, in addition to calcium alginate and CaCl2, dispersions of non-stoichiometric polyelectrolyte complexes with excess anionic groups obtained through electrostatic interactions between zein and sodium alginate or chondroitin sulfate to the crystallization medium.

Chapter 6 presents an original approach that led to the development of functional textiles with moisturizing properties, using bioactive oil-in-water emulsions based on macerated *Daucus Carota* oil and xanthan gum polysaccharide. This study aims to optimize the formulation of emulsions by varying the content of one of the components and keeping the others constant, in order to find the right conditions for obtaining stable emulsions that are compatible with application on the skin. Stable emulsions are tested for biocompatibility and antimicrobial effects, and those that demonstrate biocompatibility are tested—either as such or on textiles—as skin care products, with a focus on skin moisturizing properties and comfort indices.

The doctoral thesis concludes with a series of general conclusions and perspectives for the development of the proposed studies, accompanied by two Annexes organized as follows: Annex 1 – Dissemination of scientific results and Annex 2 – Copies of published articles.

PART II. ORIGINAL RESULTS

3. Micro- and nanostructured biomaterials based on polysaccharides, in the form of interpolymeric complexes

3.1. Preparation and characterization of non-stoichiometric interpolymeric complexes based on polysaccharides and other natural polymers

3.1.1. Characterization of zein solutions/dispersions

To study the solubilization capacity of the zein used in this study, solutions with alcohol concentrations in water ranging from 60 to 90% (denoted Zx, x = ethanol concentration) were prepared. The mean hydrodynamic diameter, D_h , and the intensity of scattered light, I, were measured at a pH between 2 and 9 (Figure 3.1).

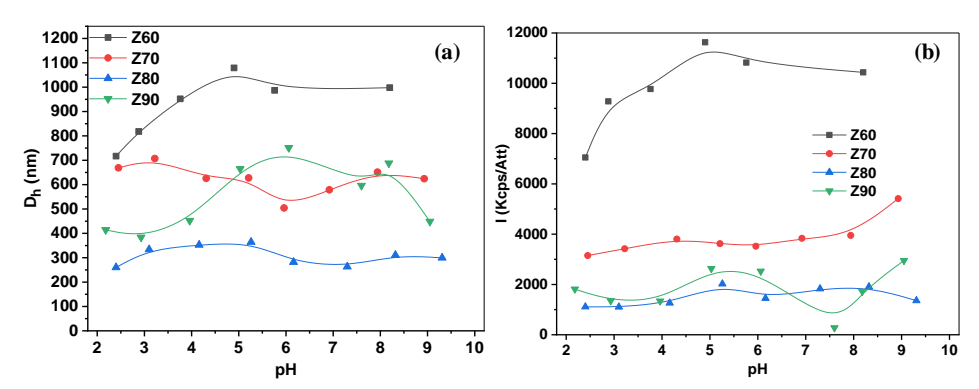


Figure 3.1. Variation in average hydrodynamic diameter (Dh) (a) and scattered light intensity (I) (b) for zein solutions with alcohol concentrations between 60 and 90%, as a function of solution pH (Lotos, 2024a).

As can be seen in Figure 3.1, both the alcohol/water ratio and the pH influenced the characteristics of the zein solutions/dispersions, with D_h decreasing as the alcohol content in water increased. Increasing the alcohol concentration to 80% and 90%, respectively, led to a decrease in D_h (Figure 3.1a), but two or even three particle populations are observed in the size distribution. A general observation is that, for the same alcohol/water ratio, the pH variation does not significantly influence the dimensional distribution and D_h value for the four alcohol/water ratios studied. At the same time, the values of scattered light intensity (Figure 3.1b), which are proportional to the mass of the aggregates, are less influenced by

the pH value, the alcohol content being the main parameter for ranking the intensity, with the highest values found for a lower alcohol content, while lower and almost similar values were found for Z80 and Z90, respectively.

The variation of the apparent zeta potential (ζ_{app}) as a function of pH for zein solutions with different alcohol concentrations and for the two polysaccharides (ANa and CSA) is shown in Figure 3.5.

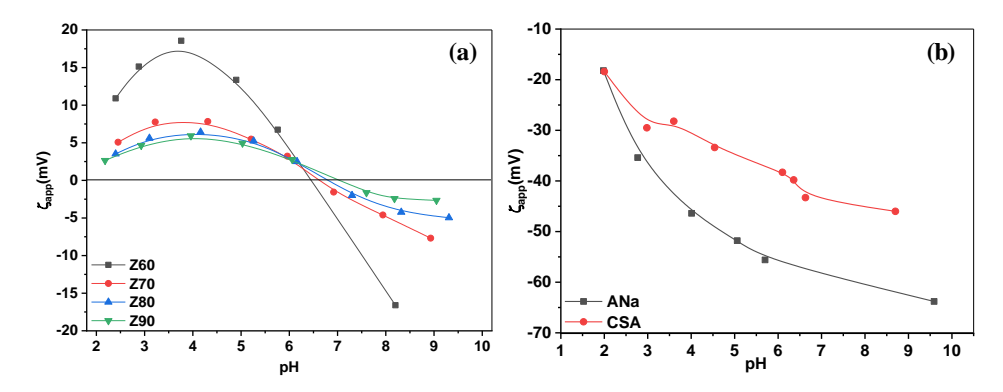


Figure 3.5. Variation of apparent zeta potential (ζ_{app}) for zein solutions with different alcohol concentrations (a) and two polysaccharide solutions (b), depending on the pH value of the solution (Lotos, 2024a).

For the same alcohol content, zein changes its positive or negative ionic charge (ζ_{app}) depending on the pH of the solution, as shown in Figure 3.5a. Thus, the zein used in this study, consisting predominantly of α -zein, depending on the alcohol concentration in the solution, has an isoelectric point at pH values of approximately 6.4–7.0; at a pH lower than this, zein is positively ionically charged. In the case of ANa and CSA polysaccharides, they are negatively charged across the entire pH range tested (Figure 3.5b).

Since the aim of this study was to obtain interpolymeric complexes and taking into account the complementary characteristics of the polymers in solution, pH = 4 was chosen, at which zein in 60% (Z60) and 70% (Z70) alcohol solutions is positively ionically charged, complementary to the negative ionic charges of both polysaccharides.

3.1.3. Nanoparticles of zein/polysaccharide complexes

In an attempt to reduce particle size, the reverse order of addition was tested, this time with the titrate being the polysaccharide and the titrant being zein (Figure 3.9). Thus, when zein was the titrant, the particle size was approximately 100 nm up to a molar ratio of 1.2, with nearly monodisperse particles obtained (Figure 3.9d, polydispersity index below 0.2). Most likely, the titrated polysaccharide was able to easily incorporate the more concentrated zein under the experimental conditions applied. Figure 3.9c illustrates a large increase in scattered light intensity when the molar ratio of charges increased above 0.8,

simultaneously with an increase in particle size. It can be assumed that the polysaccharide chains rapidly incorporate the zein dispersion, and even though the zeta potential values are still negative and suggest that stoichiometry is not reached, it should be noted that these values are only given by the anionic groups available on the NPEC surface (Figure 3.9a).

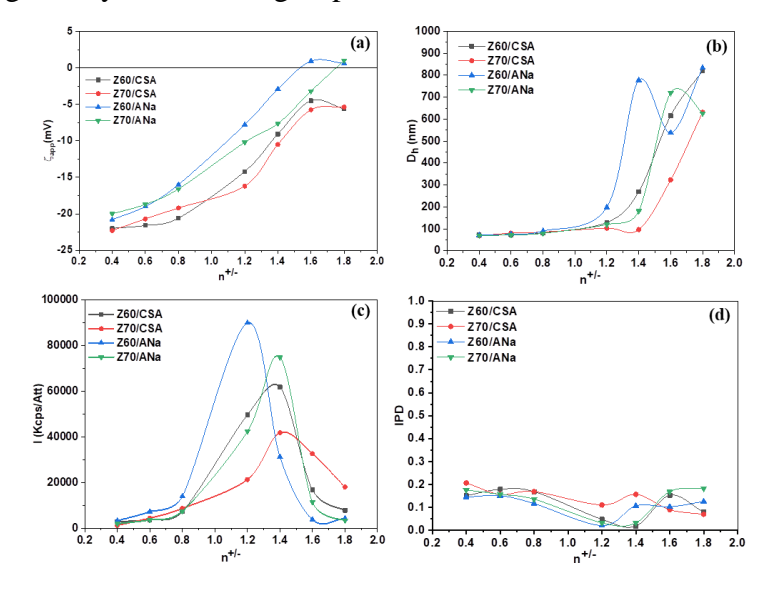


Figure 3.9. (a) Apparent zeta potential (ζ_{app}), (b) mean hydrodynamic size (D_h), (c) scattered light intensity, and (d) polydispersity index (PDI) of zein/polysaccharide CPN (addition rate = 0.08 mL/min) (Lotos, 2024a).

The size and shape of the nanoparticles obtained when zein was the titrant were also monitored by SEM (Figures 3.13 and 3.14). Thus, the analyzed nanoparticles are mainly spherical in shape (especially for CSA-based samples), along with some irregularly shaped or agglomerated structures, with slightly smaller dimensions than those resulting from DLS measurements, probably due to water removal during drying. Also, the color contrast at the edges of the particles suggests the formation of core/shell structures, supporting the hypothesis that the polysaccharide incorporated zein, based on the ζ_{app} values.

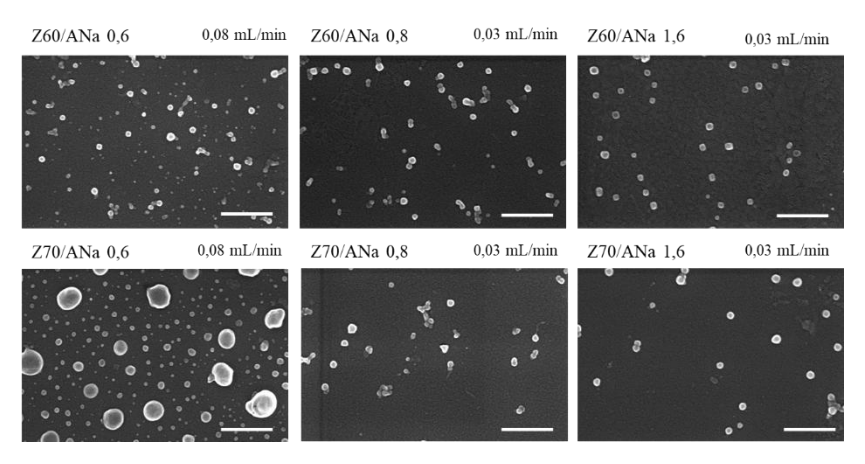


Figure 3.13. SEM micrographs of zein/ANa nanoparticles with different polymer ratios, different addition rates, and different alcohol/water content in zein solutions (scale 500 nm) (Lotos, 2024a).

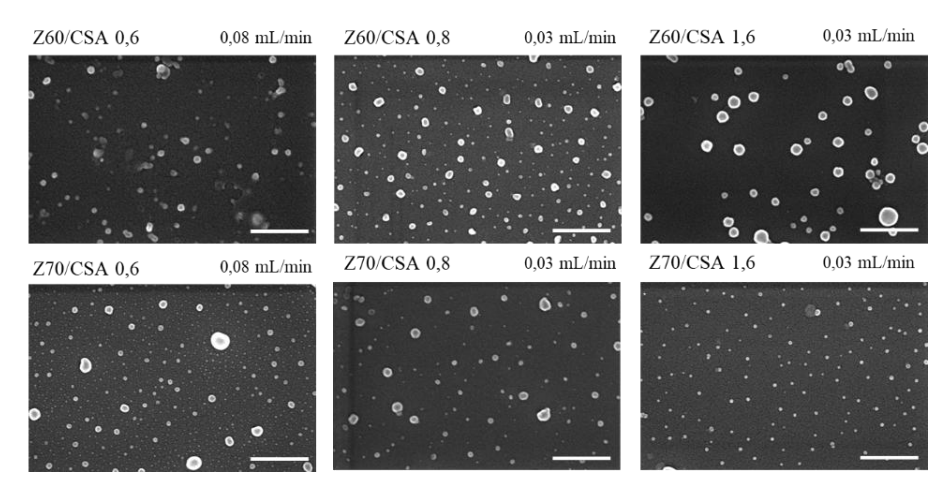


Figure 3.14. SEM micrographs of zein/CSA nanoparticles with different polymer ratios, different addition rates, and different alcohol/water content in zein solutions (scale 500 nm) (Lotos, 2024a).

3.1.4. Nanoparticles of zein, polysaccharides, and ciprofloxacin complexes

Taking into account the results presented in the previous subchapters, two NPEC samples with similar zeta potential values (approximately -20 mV, Figure 3.11a) were selected, namely those with $n^{+/-} = 0.8$, addition rate of 0.03 mL/min, Z70, and both polysaccharides to be tested for obtaining three-component complexes through the interaction of preformed NPEC with CF. The characteristics of CF/NPEC particles, depending on CF content, are shown in Figure 3.18, while their morphology is shown in Figure 3.19.

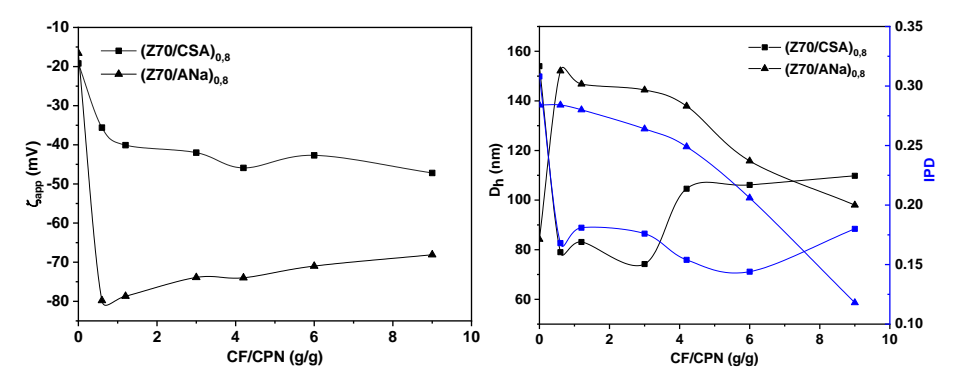


Figure 3.18. Variation of zeta potential, hydrodynamic diameter (D_h) , and polydispersity index (PDI) of CF/NPEC nanoparticles as a function of CF content (Lotos, 2024a).

The zeta potential for CSA-based CF/NPEC has higher negative values (approximately -40 mV) compared to that obtained for the corresponding nanoparticles without CF (approximately -20 mV), regardless of the CF content. On the other hand, for ANa-based NPEC, the presence of CF leads to zeta potential values of up to -70 mV, with absolute values decreasing slightly as CF increases. For NPEC with ANa, increasing the CF content leads to a decrease in nanoparticle size, along with a decrease in polydispersity, suggesting that CF improves the physical properties of nanoparticles by reducing their

tendency to aggregate. In comparison, for NPEC with CSA, the size of the nanoparticles increases slightly with increasing CF content, resulting in CF/ NPEC particles of up to 60 nm. Furthermore, the polydispersity index values for NPEC with CSA are below 0.2 for all samples, regardless of CF content, indicating the formation of nearly monodisperse particles. The SEM micrographs in Figure 3.19 show that the morphology of the nanoparticles did not change after interaction with CF, suggesting good incorporation of the antibiotic into the three-component complexes.

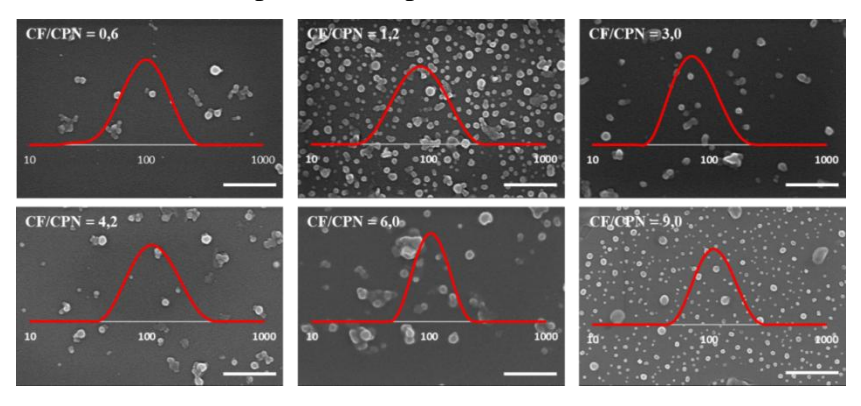


Figure 3.19. SEM images of three-component complexes formed from CSA-based NPECs with $n^{+/-}=0.8$ and different CF contents (scale 500 nm). The hydrodynamic diameter distribution of the particles determined by DLS is inserted in each image (Lotos, 2024a).

3.1.6. Study of the antibacterial activity of modified surfaces

To comparatively evaluate the antibacterial activity, NPEC and CF/NPEC nanoparticles were deposited on the NWM surface, their adhesion being the result of electrostatic and hydrophobic interactions. For comparison, a sample was prepared in which the NWM material was coated only with zein. The results obtained in the tests on the antibacterial properties of the original nonwoven material and those with Z70, NPEC, or CF/NPEC are shown in Figure 3.23 and Table 3.2.

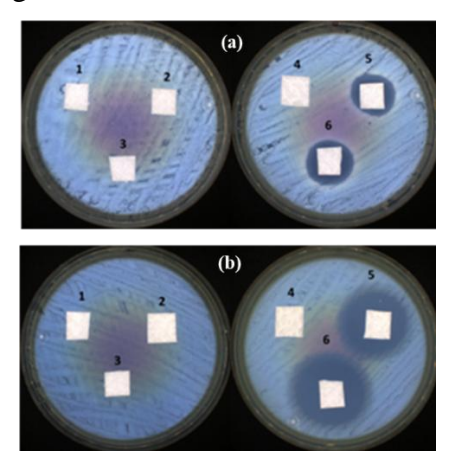


Figure 3.23. Antibacterial activity against (a) S. aureus and (b) E. coli of material treated with Z70, NPEC, or CF/NPEC (see sample number correspondence in Table 3.2) (Lotos, 2024a).

Table 3.2. Antibacterial activity of the tested samples against the reference strains S. aureus and E. coli (mm) (Lotos, 2024a).

Sample No.	Comple code	Inhibition zone (mm)			
	Sample code	S. aureus	E. coli		
1	NWM	-	-		
2	$NWM + Z70 \ 10^{-4} \ M$	-	-		
3	$NWM + (Z70/ANa)_{0.8}$	-	-		
4	$NWM + (Z70/CSA)_{0.8}$	-	-		
5	$NWM + (Z70/ANa)_{0.8} + CF 15 ml$	21.35 ± 2.33	25.15 ± 1.20		
6	$NWM + (Z70/CSA)_{0.8} + CF 15 ml$	20.10 ± 0.57	27.75 ± 1.20		

As can be seen in Figure 3.23, the initial cellulose material, as well as the samples containing Z70 or NPEC, have no antibacterial activity due to their excellent biocompatibility properties (Vasiliu, 2022). In contrast, the samples with antibiotics showed antibacterial activity (up to 27 mm inhibition zone against *E. coli* in the case of NPEC with CSA and ciprofloxacin). It is well known that ciprofloxacin is highly effective against Gram-negative bacteria and moderately effective against Gram-positive bacteria (Campoli-Richards, 1988). This is consistent with the antibacterial test performed in this study, CF/NPEC having a larger inhibition zone for *E. coli* than for *S. aureus*, regardless of the polysaccharides involved (CSA or ANa).

3.2. Preparation and characterization of interpolymeric complexes based on polysaccharides and synthetic polymers

3.2.1. Study of the physicochemical properties of Chit/PNIPAM complexes

As can be seen in Figure 3.24a, the scattered light intensity for the Chit_L/PNIPAM_L series gradually increases with increasing PNIPAM_L concentration. Since the intensity of scattered light is proportional to the mass of complexes in solution, the observed increase confirms that complexation between the two components has occurred, and the mass of complexes effectively increases as more PNIPAM_L is added. At the same time, the scattered light intensity for the Chit_S/PNIPAM_L series also shows a similar upward trend, but with higher overall values, suggesting that the particles formed in this case have a higher mass or a denser conformation.

Regarding the actual charge of the complexes, the measured zeta potential values are shown in Figure 3.24b for both the Chit_L/PNIPAM_L and Chit_S/PNIPAM_L series. Obviously, although no significant changes are observed with increasing PNIPAM_L concentration for both series, the zeta potential values of the complexes are considerably

lower than those of the corresponding chitosan samples, thus confirming the complexation between the two macromolecular components. This decrease is more pronounced in the case of samples from the Chits/PNIPAM_L series, with the zeta potential values of the complexes being close to zero, indicating the neutralization of most of the opposite charges. Regarding the size of the complexes, Figures 3.24c and 3.24e show that, for the Chit_L/PNIPAM_L series, two main populations can be distinguished, their size (approximately 30 and 220 nm, respectively) being more or less the same, regardless of the amount of PNIPAM in the complexes. These peaks indicate the presence of two different populations in the complex dispersions, which most likely correspond to particles with a different number of chains included in the complexes. A small peak at approximately 10 nm (Peak 1) is also detected for samples (Chit_L/PNIPAM_L)_{4/2} and (Chit_L/PNIPAM_L)_{4/4} and may indicate the presence of uncomplexed synthetic polymer chains, as it coincides with the corresponding peak of the PNIPAM_L sample.

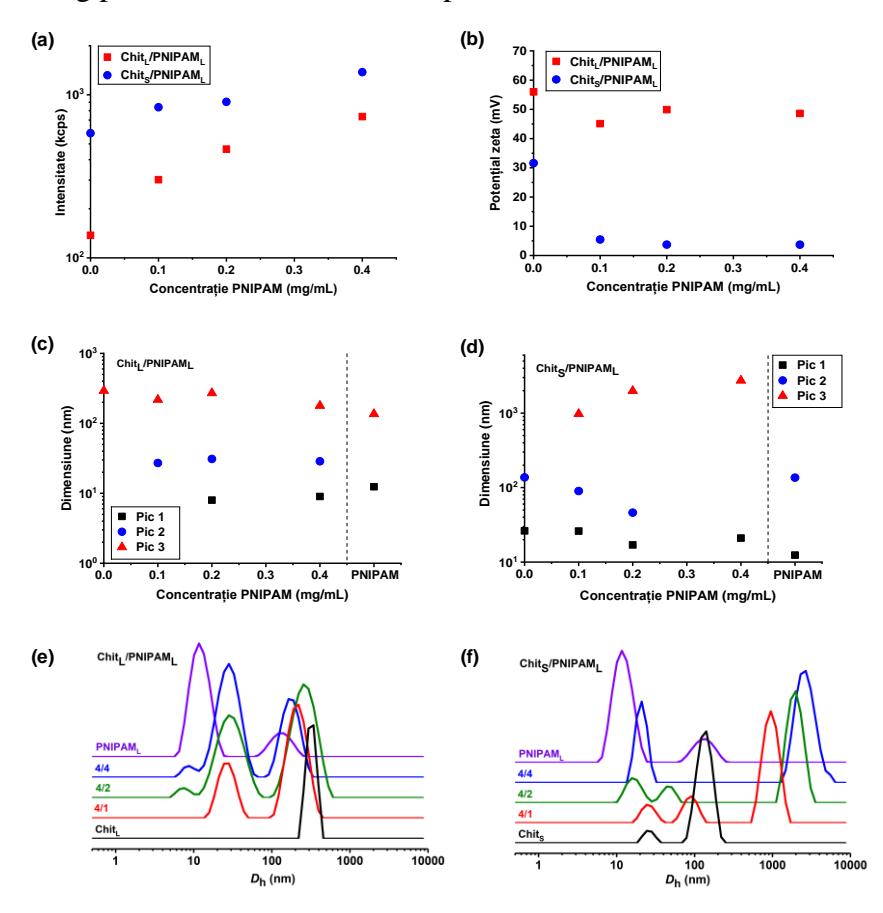


Figure 3.24. (a) Scattered light intensity, (b) zeta potential, and (c, d) peak size, derived from size distributions (e, f), for the Chit_L/PNIPAM_L and Chit_S/PNIPAM_L series. Also, for comparison, the size distributions for the Chit_L, Chit_S, and PNIPAM_L samples are included (Lotos, 2025).

For the Chit_S/PNIPAM_L series of complexes, the shorter chain chitosan also exhibits self-assembly in solution, with two peaks of approximately 25 and 150 nm observed in

Figure 3.24f, corresponding to both individual chains and multi-chain aggregates. At the same time, the size distribution of samples (Chits/PNIPAM_L)_{4/1} and (Chits/PNIPAM_L)_{4/2} shows three peaks, the size of the first two being slightly smaller than that of the peaks corresponding to the Chits sample. The results suggest that both individual chains and aggregates of multiple chains of short-chain chitosan interact electrostatically with PNIPAM chains, forming complexes that are slightly smaller than the original chitosan, as a result of reduced electrostatic repulsions due to charge neutralization and increased hydrophobic interactions caused by PNIPAM incorporation.

3.2.2. The behavior of Chit/PNIPAM complexes at different temperatures

Since PNIPAM is a thermosensitive polymer, it is expected to impart the same characteristics to Chit/PNIPAM complexes, and for this reason, the influence of temperature on the characteristics of the formed complexes was investigated. Specifically, their response to temperature was examined by performing DLS measurements at different temperatures between 25 and 45 °C (with a 5 °C increment), and the results obtained regarding the scattered light intensity, peak sizes, and corresponding size distributions are shown in Figures 3.36 and 3.37. For all samples investigated, after heating to 45 °C, the temperature was reduced to 25 °C, and the sample was measured again to examine the reversibility of the structures formed by the heating process.

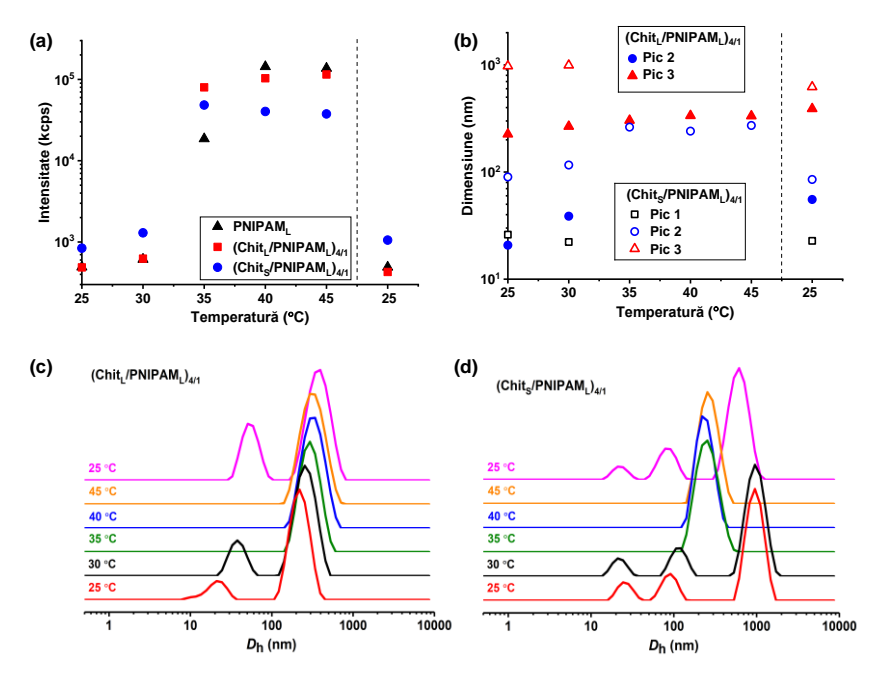


Figure 3.36. Effect of temperature on (a) scattered light intensity and (b) peak size, derived from size distributions (c, d), for samples ($Chit_L/PNIPAM_L$)_{4/1} and ($Chit_S/PNIPAM_L$)_{4/1} (Lotos, 2025).

Figures 3.36a and 3.37a show the influence of temperature on the scattered light intensity for the complexes obtained with both chitosan samples at a volume ratio of 4/1

compared to the corresponding PNIPAM samples. At 35 °C (i.e., above the LCST of PNIPAM), a sharp increase in intensity is observed, accompanied by a significant increase in turbidity for all samples. This behavior is characteristic for the phase transition of PNIPAM, attributed to the increase in hydrophobic interactions that induce aggregation between chains, and is common to all investigated samples of Chit/PNIPAM complexes. A further increase in temperature to 45 °C does not appear to have a significant effect on the intensity of the scattered light, while the initial values are completely restored after cooling to 25 °C, demonstrating the reversibility of the transition. At the same time, the size distributions for the 4/1 complexes in all four systems (Figures 3.36 c,d and 3.37 c,d) show the same transition from two or three peaks to a single peak above a temperature of 35 °C, which is also a characteristic feature of both PNIPAM samples.

This behavior suggests the aggregation of the initial populations of complexes into compact structures, due to the increased hydrophobicity of the complexed PNIPAM chains, which in turn promote interactions between chains.

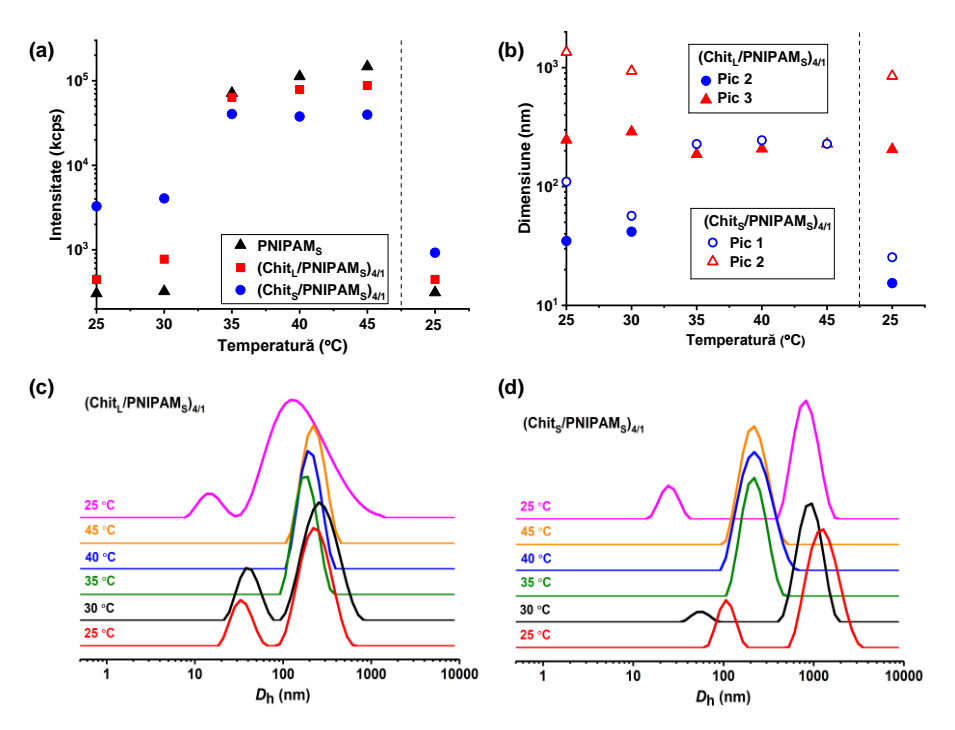


Figure 3.37. Effect of temperature on (a) scattered light intensity and (b) peak size, derived from size distributions (c, d), for samples (Chit₁/PNIPAM₅ / Chit₅/PNIPAM₅)_{4/1} (Lotos, 2025).

3.2.4. The ability to load bioactive molecules into Chit/PNIPAM complexes

The potential of Chit/PNIPAM hybrid nanostructures to be used as delivery systems for bioactive molecules was explored by examining their ability to encapsulate a natural hydrophobic compound, namely curcumin (CRC). Among the Chit/PNIPAM complexes, (Chit_L/PNIPAM_L)_{4/4} was chosen for CRC encapsulation because the combination of Chit_L

and PNIPAM_L is considered to be the most stable, while the higher amount of PNIPAM should improve the interaction with the hydrophobic bioactive molecule. Three different drug loading ratios were investigated by adding 2.5, 5, and 10% w/w of CRC relative to the total mass of the complex at 40 $^{\circ}$ C to take advantage of the phase transition of the PNIPAM chains.

The physicochemical properties of the CRC-loaded samples (Chit_L/PNIPAM_L)_{4/4} were investigated by performing DLS measurements on 1:10 diluted solutions, and Figure 3.49 shows the scattered light intensity values and peak sizes resulting from the size distributions.

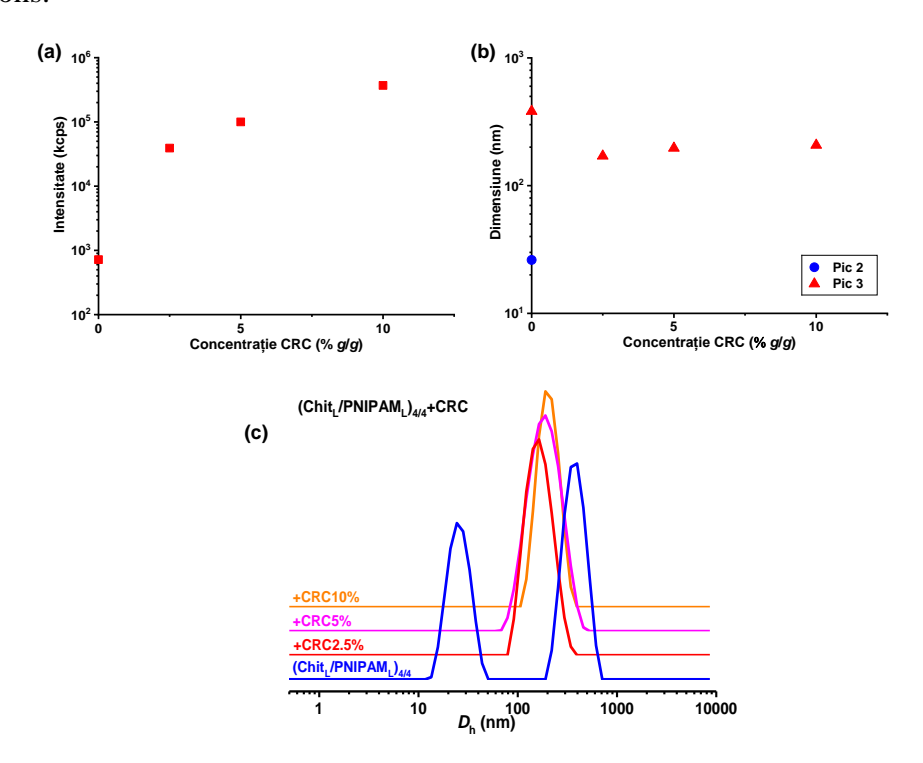


Figure 3.49. DLS results in terms of (a) scattered light intensity and (b) peak size, derived from (c) size distributions, for samples of ($Chit_L/PNIPAM_L$)_{4/4} loaded with CRC (Lotos, 2025).

The DLS results show that the (Chit_L/PNIPAM_L)_{4/4} sample loaded with CRC exhibits a pronounced increase in scattered light intensity, indicating a larger mass of structures (Figure 3.49a). In terms of the size of the complexes loaded with bioactive molecules, a transition is detected from the two peaks identified for the initial complex to a single peak with an intermediate size, which is accompanied by a significant decrease in the polydispersity index (i.e., from approximately 0.6 to 0.1). The observed changes confirm the successful incorporation of CRC and further suggest a reduction in the size of the initial complexes and the formation of more compact/dense structures as a result of increased hydrophobic interactions due to the presence of CRC molecules. However, the effective positive charge of the primary Chit/PNIPAM complexes is maintained, with the

sample with the highest CRC concentration ((Chit_L/PNIPAM_L)_{4/4}+10% CRC) exhibiting a zeta potential value of approximately +30 mV.

To determine the concentration of encapsulated CRC, UV-Vis spectroscopic measurements were performed, and the spectra obtained are shown in Figure 3.50a, together with the corresponding spectrum of (Chit_L/PNIPAM_L)_{4/4}, for comparison. From the absorbance values obtained at 427 nm and using the CRC calibration curve made in ethanol (Figure 3.50), the concentration of CRC encapsulated in the complex solutions/dispersions was calculated. The corresponding values for each loading ratio are presented in Table 3.5, together with the added CRC concentration and the encapsulation efficiency calculated with equation (2.8) (Chapter 2).

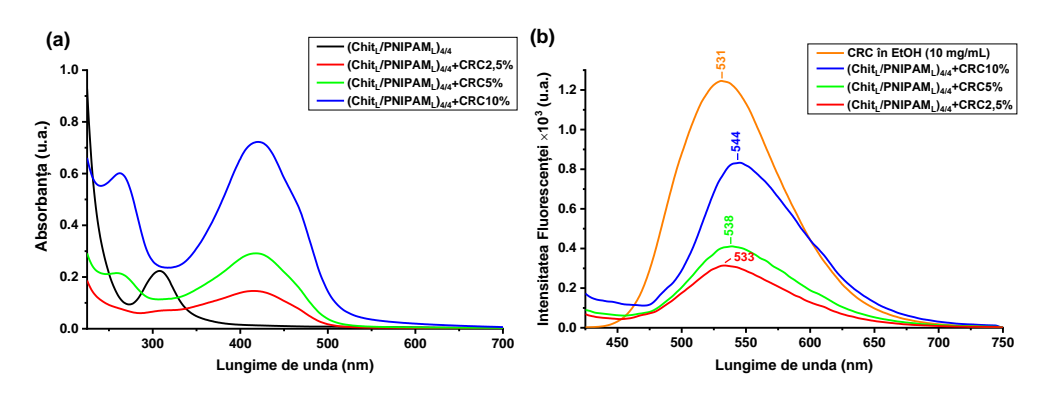


Figure 3.50. (a) UV-Vis spectra and (b) fluorescence spectra for (Chit_L/PNIPAM_L)_{4/4} samples loaded with CRC (Lotos, 2025).

Table 3.5. Concentration of added and encapsulated CRC, together with encapsulation efficiency EE%, for (Chit_L/PNIPAM_L)_{4/4} samples loaded with CRC (Lotos, 2025).

Codul probei	C _{CRC} adăugată (μg/mL)	C_{CRC} încapsulată ($\mu\mathrm{g/mL}$)	EE%
(Chit _L /PNIPAM _L) _{4/4} +2,5% CRC	19,6	8,5	43,4
(Chit _L /PNIPAM _L) _{4/4} +5% CRC	38,5	17,9	46,5
(Chit _L /PNIPAM _L) _{4/4} +10% CRC	74,1	45,4	61,3

The estimated EE% values range between 43 and 61% for the three CRC concentrations investigated (2.5, 5, and 10% w/w), indicating sufficient loading capacity of the bioactive molecule for the complex formed between Chit_L and PNIPAM_L, which is undoubtedly correlated with the overall hydrophobicity of the system. Fluorescence spectroscopy was used to verify the fluorescent properties of CRC-loaded complexes and, thus, their potential use in applications relevant to bioimaging. Figure 3.50b shows the spectra obtained for the three different CRC concentrations investigated, together with the corresponding spectrum of CRC in ethanol (at a concentration of 10 μ g/mL). Compared to the CRC spectrum, an apparent gradual shift towards red of the characteristic CRC peak from 531 to 544 nm can be observed for complexes loaded with the bioactive molecule.

This shift is attributed to the hydrophobic interactions of CRC with the PNIPAM chains (especially since the loading procedure was performed above the LCST value) (Selianitis, 2022; Skandalis, 2022), although it is possible that the hydrophobic regions of the chitosan backbone also facilitate CRC encapsulation.

4. Micro- and nanostructured biomaterials based on grafted chitosan, in the form of polyplexes

4.1. Preparation and characterization of chitosan-*g*-poly(*N*-isopropylacrylamide) copolymer

4.1.1. Characterization of the Chit-g-PNIPAM copolymer

The reaction mechanism proposed for chitosan grafting with PNIPAM is described in Figure 4.1. In the first stage, the KPS initiator, decomposed under the influence of temperature, can extract an H atom from the amino group of chitosan, generating a stable salt (potassium bisulfate) and two radicals in the system, the amino radical from chitosan and the bisulfate radical from KPS. The latter, which is more reactive than the polymeric radical, can attack the PNIPAM chain at the active tritiocarbonate terminal group, forming a PNIPAM macroradical (step 2). This macroradical can further react with the chitosan radical to form the graft copolymer Chit-g-PNIPAM (step 3).

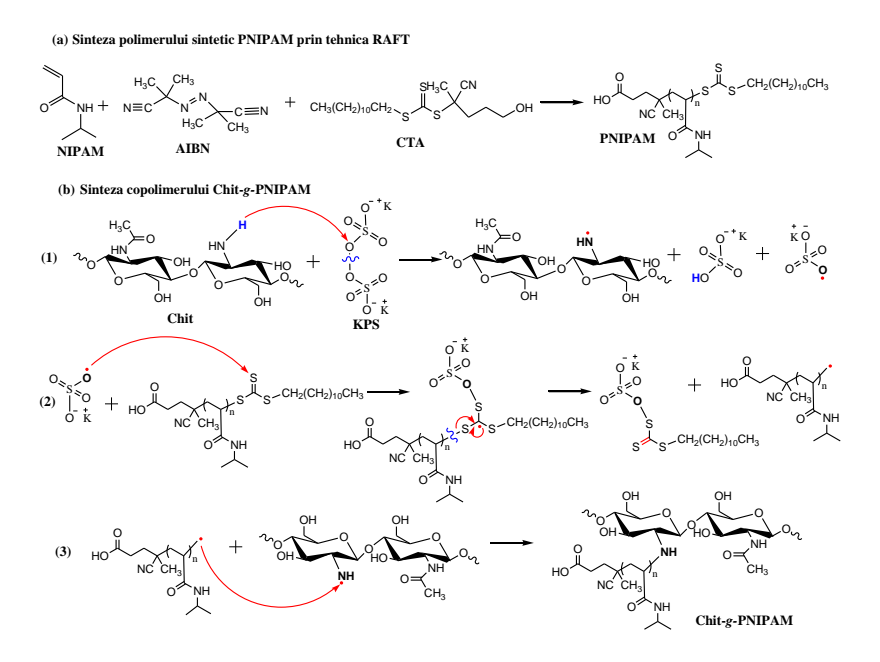


Figure 4.1. Schematic representation of (a) PNIPAM synthesis by RAFT polymerization and (b) the proposed mechanism of PNIPAM grafting onto chitosan: (1) KPS extracts an H atom from the amino group of chitosan, generating chitosan and bisulfate radicals; (2) the bisulfate radical attacks PNIPAM at the active tritiocarbonate terminal group, generating a macroradical; (3) the PNIPAM macroradical reacts with the NH• radical on chitosan (Zaharia, 2024).

4.1.1.1. FTIR-ATR spectroscopy

The obtained Chit-*g*-PNIPAM copolymer was validated by FTIR-ATR spectroscopy (Figure 4.2). Thus, the stretching vibration of the N-H group in PNIPAM was identified at 3292 cm⁻¹ (Rwei, 2016). In addition, the stretching vibration of carbonyl (amide I) was observed at 1641 cm⁻¹ and the bending vibration of N-H (amide II) at 1537 cm⁻¹ (Ziminska, 2020). The isopropyl group in PNIPAM in the FTIR-ATR spectrum shows characteristic bands at 2971 cm⁻¹ and 2933 cm⁻¹ corresponding to the -CH (symmetric and asymmetric), as well as two bands at the wave numbers 1371 cm⁻¹ and 1461 cm⁻¹, attributed to the -CH₃ group.

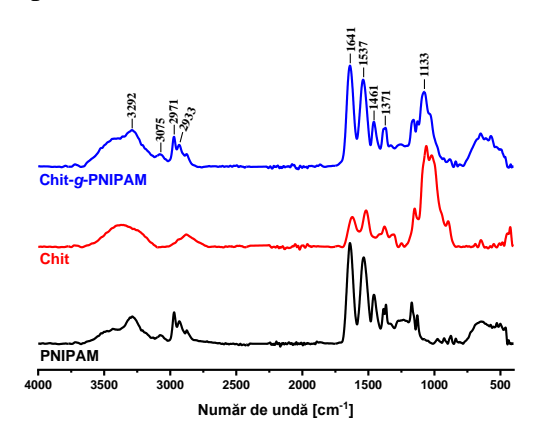


Figure 4.2. FTIR-ATR spectra of PNIPAM, chitosan, and Chit-g-PNIPAM (Zaharia, 2024).

The band at 1133 cm⁻¹ was correlated with the C-O stretching vibration in chitosan, indicating its presence in the copolymer structure. The characteristic bands of N-acetyl groups in the chitosan structure are present at approximately 1618 cm⁻¹ (C=O, amide I) and 1325 cm⁻¹ (C-N, amide III), and overlap with those of PNIPAM. Signals characteristic of both PNIPAM and chitosan were identified in the FTIR-ATR spectrum of the graft copolymer. Furthermore, the copolymer does not contain sulfur atoms in its structure, as evidenced by the FTIR-ATR spectrum by the disappearance of the bands at 860 and 610 cm⁻¹ in the Chit-*g*-PNIPAM spectrum, which were attributed in the PNIPAM spectrum to the tritiocarbonate group.

4.1.1.3. Thermogravimetric analysis

The thermogravimetric analysis of chitosan, PNIPAM, and Chit-g-PNIPAM was performed in the temperature range of 37–700 °C, and the thermal behavior (mass loss) was evaluated by comparison (Figure 4.4). Chitosan and PNIPAM showed different thermal degradation profiles, with PNIPAM exhibiting greater thermal stability until its complete decomposition at 450 °C. The TG curve of chitosan showed two stages of decomposition (Figure 4.4, dashed line). The first stage occurred in the temperature range

of 38–96 °C and was due to water loss (Kumar, 2012), with a mass loss of approximately 9.58%. Major decomposition began at 150 °C with a mass loss of approximately 44% and was caused by dehydration of the pyranose cycles, then depolymerization, followed by thermal degradation of the polysaccharide chain (Sosnik, 2015).

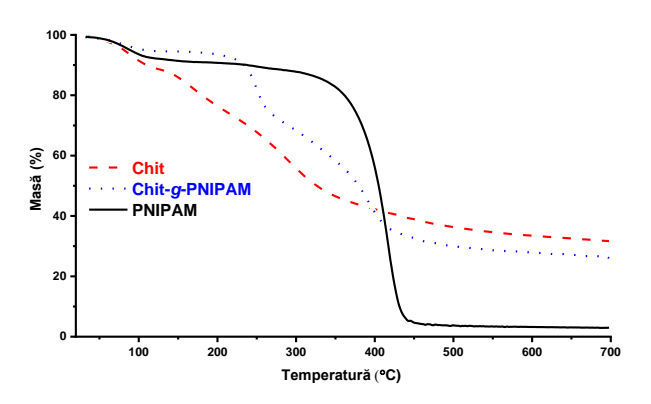


Figure 4.4. Thermogravimetric curves for chitosan, PNIPAM, and Chit-g-PNIPAM (Zaharia, 2024).

The degradation of PNIPAM was also limited to two stages (Figure 4.4, straight line): the first stage, which was detected at approximately 93 °C, included an 8% mass loss and may be due to water evaporation, and the second stage between 350 and 450 °C can be attributed to the complete thermal degradation of the synthetic polymer. At the same time, for the Chit-g-PNIPAM copolymer, the degradation process took place in three stages (Figure 4.4, dotted line). The first stage, at approximately 95 °C and accompanied by a 4% mass loss, was attributed to the evaporation of water present in the copolymer, which was retained by the formation of hydrogen bonds with it. The decomposition of the chitosan polysaccharide chain is responsible for the second mass loss (26%) in the temperature range of 200–300 °C. The third stage, which begins at 310 °C, with a mass loss of 35%, was attributed to the thermal decomposition of the synthetic PNIPAM chain. The thermal stability of chitosan in the graft copolymer decreased from 250 to 210 °C due to the impact of PNIPAM on the crystalline phase of chitosan (Queiroz, 2014). These thermal changes occur at temperatures that are not relevant to possible medical applications and will never be encountered *in vivo*.

4.1.2. The influence of temperature on the properties of Chit-g-PNIPAM solutions

The influence of the heating/cooling process (in the temperature range 25–45 °C) on all indicated parameters is shown in Figure 4.6. The temperature range used for measurements was determined based on the properties of PNIPAM, which has an LCST of approximately 32 °C.

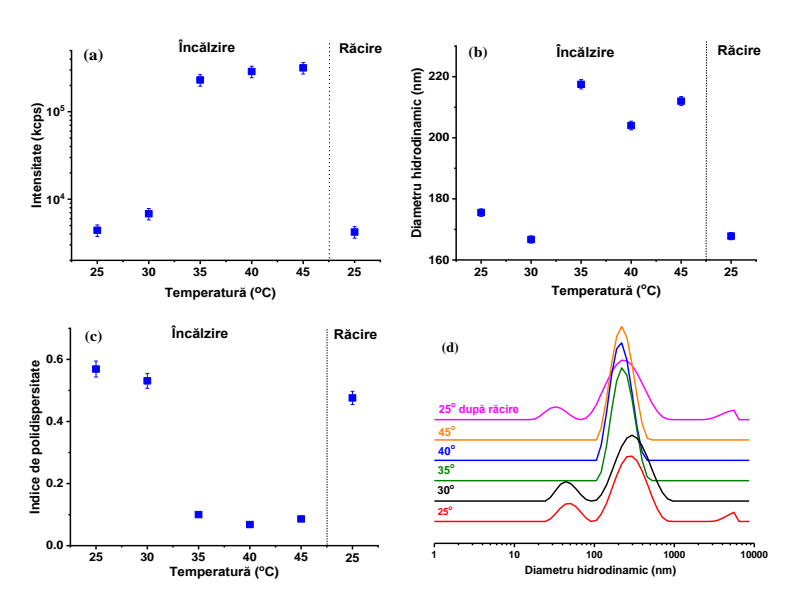


Figure 4.6. Influence of temperature on (a) scattered light intensity, (b) hydrodynamic diameter, (c) polydispersity index, and (d) size distribution of Chit-g-PNIPAM (polymer concentration: 1.2 mg/mL; pH = 6.5) (Zaharia, 2024).

From Figure 4.6a, it can be seen that the increase in temperature has an impact on the mass of Chit-g-PNIPAM aggregates, as evidenced by the increase of scattered light intensity above the LCST of PNIPAM. Also, the hydrodynamic diameter of the Chit-g-PNIPAM particles varied with temperature, suggesting that particles already formed at low temperature combine with each other as the temperature rises above the LCST, changing their density and size as the temperature increases (Figure 4.6b). This occurs in parallel with an increase in aggregate mass, as indicated by the increase in intensity. This process can be attributed to the generation of more compact structures through the dehydration of PNIPAM chains, based on hydrophobic interactions between the hydrophobic parts of Chit-g-PNIPAM and H bonds between the amide groups in PNIPAM and the hydroxyl groups in chitosan. Figure 4.6c illustrates that the polydispersity index values are greater than 0.2 at temperatures below LCST and decrease below 0.2 at temperatures above LCST, suggesting a transition from disordered structure to more ordered/dense aggregates of Chit-g-PNIPAM (Bao, 2010). The size distribution for the Chit-g-PNIPAM copolymer (Figure 4.6d) demonstrates that at temperatures above 35°C, where the grafted PNIPAM chains possess increased hydrophobicity, there is a single population. After cooling the Chit-g-PNIPAM solutions, the reversibility of the aggregation/solubilization process was demonstrated, as can be seen in Figure 4.6 (last point in the diagrams, after cooling to 25 °C), with the size of the Chit-g-PNIPAM particles, the polydispersity index, and the scattering light intensity returning approximately to their initial values at 25 °C. Therefore, the thermosensitive properties of the newly synthesized Chit-*g*-PNIPAM copolymer recommend it as a potential candidate for the construction of smart nanocontainers for the subsequent release of bioactive compounds (e.g., as a "smart" gene delivery system).

4.2. Preparation and characterization of Chit-g-PNIPAM and DNA-based polyplexes

4.2.1. Physical and chemical properties of Chit-g-PNIPAM/DNA polyplexes

The results obtained in terms of scattered light intensity, hydrodynamic radius (R_h) values of the different populations identified, highlighted by different peaks in the size distribution functions, together with the zeta potential of the polyplexes are presented in Figure 4.7, depending on the N/P ratio.

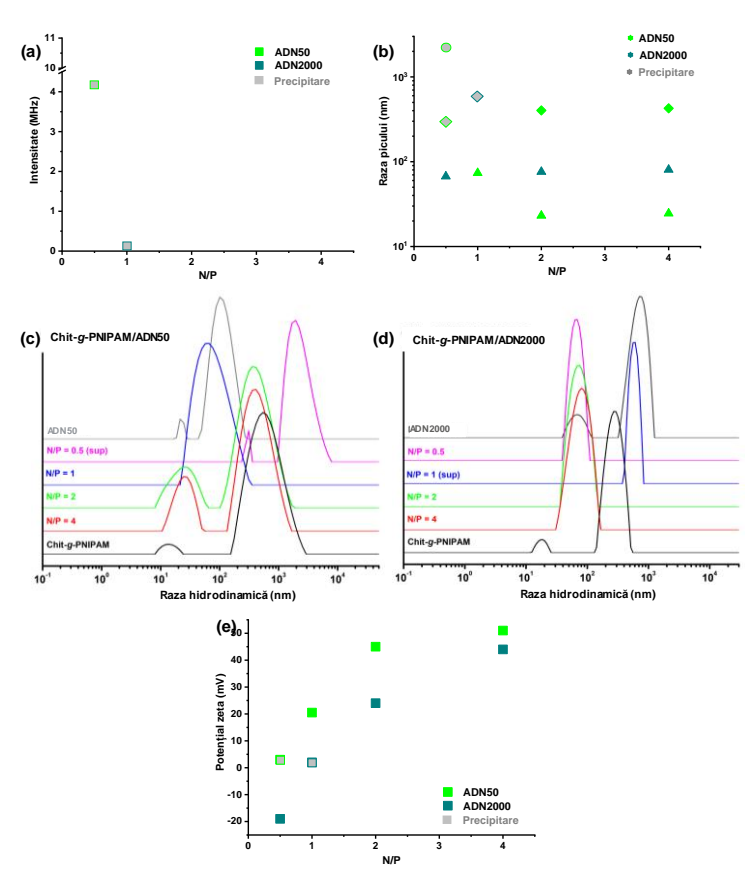


Figure 4.7. DLS and ELS results regarding (a) scattered light intensity, (b) hydrodynamic radius, (c, d) size distribution, and (e) zeta potential values for Chit-g-PNIPAM/ADN50/2000 polyplexes (Karayianni, 2024).

As can be seen in Figure 4.7a, the mass (which is directly proportional to the intensity of scattered light) of the polyplexes formed between the graft copolymer Chit-g-PNIPAM and DNA shows the highest values for N/P ratios below 1 (i.e., the estimated charge neutralization point). Therefore, it can be deduced with reasonable certainty that, for N/P \leq 1, the interaction between the two components is extremely strong or, in other words, the excess of DNA relative to the available amino groups of

Chit-g-PNIPAM leads to the formation of polyplexes or large aggregates. When the Chit-g-PNIPAM copolymer is in excess and, therefore, there is a surplus of positive charges, i.e., for N/P > 1, the resulting polyplexes are less dense and are colloidally stable. Finally, it is worth noting that, for the same N/P values, the polyplexes formed with DNA2000 have a higher mass or are denser than those with DNA50, which may indicate a higher degree of interaction with the grafted copolymer.

Regarding the size of the formed polyplexes, the size distribution functions (Figure 4.7, c and d) provide valuable information. First, the Chit-g-PNIPAM solution exhibits two peaks indicating two populations in solution, with corresponding R_h values in the range of 10–20 nm and approximately 300–600 nm. The presence of the second peak indicates a certain degree of self-assembly of the graft copolymer, forming aggregates with multiple chains, most likely due to hydrophobic interactions originating from the chitosan chain or intra-polyelectrolytic interactions of the copolymer. Therefore, both Chit-g-PNIPAM copolymer chains and aggregates coexist in solution.

Regarding the Chit-*g*-PNIPAM/DNA50 polyplexes, at high N/P values (2 and 4), the size distribution functions (Figure 4.7b) are similar to those of the pure copolymer or, in other words, the sizes of the two polyplex populations are dictated by the corresponding populations of the graft copolymer that is in excess. A rather interesting aspect is that for the Chit-*g*-PNIPAM/DNA2000 system, the size distributions show a single peak (one population), with a fairly similar size of approximately 75 nm for all three stable dispersions. This indicates the formation of dense polyplexes regardless of the amount of grafted copolymer, which is obviously a direct consequence of the length of the DNA sample.

The information regarding the effective charge of the formed polyplexes, derived from the zeta potential values (Figure 4.7e), is consistent with the hypotheses formulated so far. Starting from the highest N/P value, both Chit-g-PNIPAM/ADN50/2000 systems show relatively high positive values, close to that measured for the pure copolymer, which is approximately +50 mV. This observation confirms that when the Chit-g-PNIPAM copolymer is in excess, the general properties and conformation of the polyplexes are mainly dictated by its intrinsic conformation/aggregation state and characteristics. As the N/P ratio decreases (DNA content increases), a gradual decrease in the zeta potential of the polyelectrolytes can be observed, reaching values close to zero in the case of the DNA50 sample or even negative values (i.e., charge reversal) in the case of DNA2000. This confirms that polyplexes formed at N/P ratios close to 1 are characterized by a reduced

overall charge, as a result of the neutralization of the charge that occurs during the electrostatic interaction of the two components.

To obtain additional information on the morphology of the polyplexes, STEM imaging was performed for those formed at N/P = 4 and both Chit-g-PNIPAM/ADN50/2000 systems, as can be seen in Figure 4.8.

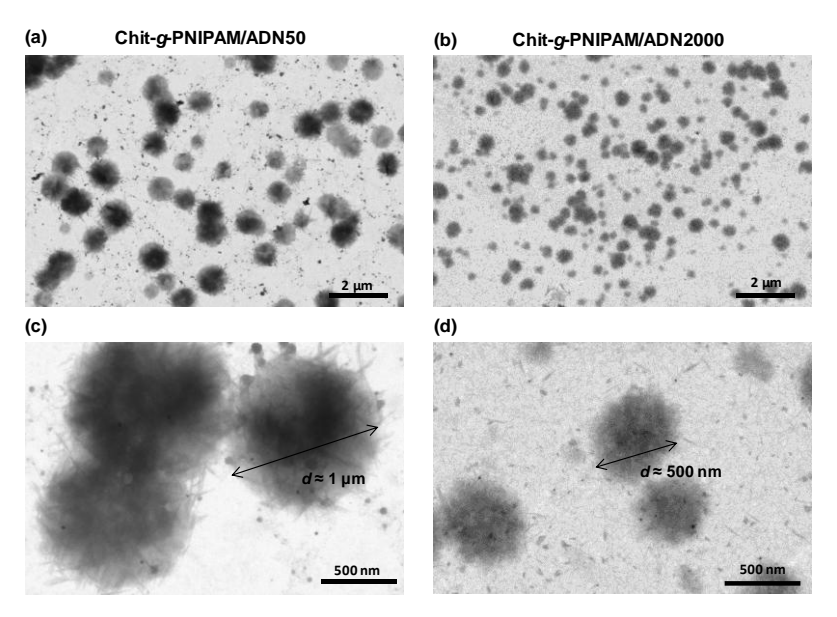


Figure 4.8. STEM images for stable polyplexes formed at N/P = 4 for both systems (a, c) Chit-g-PNIPAM/ADN50 and (b, d) Chit-g-PNIPAM/ADN2000 (Karayianni, 2024).

In both cases, homogeneous spherical nanostructures of different sizes with an urchin-like structure can be observed. Evidently, the density of the polyplexes decreases near their periphery, and in the outer parts of the formed nanostructures (especially for DNA50), straight or slightly curved structures of complexed copolymer/DNA chains are visible. This latter feature may be a result of the semi-rigid nature of both DNA and the chitosan chain and may lead to a ladder-like co-assembly of the primary DNA/grafted copolymer complexes.

4.2.2. Study of the thermal response of Chit-g-PNIPAM/DNA polyplexes

As anticipated, the presence of PNIPAM side chains confers thermosensitivity to the graft copolymer (Zaharia, 2024), which can be exploited in potential bioapplications. Therefore, investigating the thermal response of Chit-g-PNIPAM/ADN50/2000 polyplexes is of particular interest. Figure 4.9 shows the results obtained in terms of the increase in scattered light intensity and the R_h values of the different peaks identified in the corresponding size distribution functions, as a function of temperature, for both Chit-g-PNIPAM/ADN50/2000 systems. It should be noted that, in all cases, after gradually

increasing the temperature to 45 °C, the sample was cooled to 25 °C and measured again to examine the reversibility of any changes that had occurred.

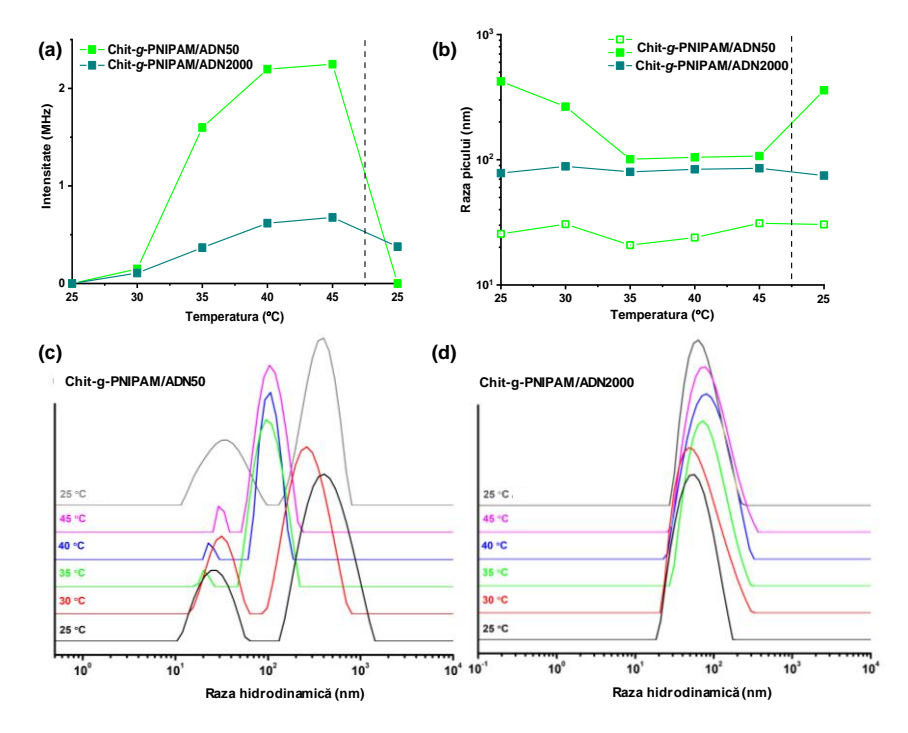


Figure 4.9. Influence of temperature on (a) scattered light intensity, (b) hydrodynamic radius, (c, d) size distribution functions for polyplexes formed at N/P = 4 for Chit-g-PNIPAM/ADN50 and Chit-g-PNIPAM/ADN2000 systems (Karayianni, 2024).

For polyplexes formed at N/P = 4, a significant increase in scattered light intensity above 35 °C is observed for both systems, as shown in Figure 4.9a, with the change being even more pronounced for polyplexes formed with the short DNA sample. At the same time, the size of DNA2000-based polyplexes does not appear to be affected by the increase in temperature, with only a slight broadening of the R_h peak observed in the corresponding size distribution functions (Figure 4.9d). On the contrary, for the DNA50 system, a considerable decrease in the larger population size is observed (Figure 4.9c), while for the smaller population size there is a much smaller decrease, observed especially at a temperature of 35 °C.

4.2.4. Stability of Chit-g-PNIPAM/DNA polyplexes in biological fluids

In addition to stability against ionic strength, it is equally important to test the behavior of polyplexes when interacting with biological fluids, as a way to simulate their response to entering the human body. For this purpose, stable polyplex dispersions of both systems were mixed (in equal volumes) with FBS solutions of different concentrations, 10 and 50% v/v in PBS, and the final equilibrated mixtures were measured by DLS first at room temperature (25 °C) and then at body temperature (37 °C) after incubation for 30

min. Figure 4.14 shows the results obtained in terms of the increase in scattered light intensity and the R_h values resulting from the corresponding size distribution functions for the polyplexes at N/P = 4 of both Chit-g-PNIPAM/ADN50/2000 systems, after mixing with FBS solutions of different concentrations (10 and 50% v/v).

The DLS results show an increase mainly in the scattering light intensity and, to a lesser extent, in the size of the polyplexes formed with DNA50 after mixing with FBS solutions, with the differences being more pronounced for the higher FBS concentration. Even after incubation at 37 °C, small changes are observed. Therefore, it can be assumed that although polyplexes interact with the components of the FBS solution (mainly proteins and enzymes), as there is a considerable increase in intensity, their size does not change very much, most likely due to their initial structure, which allows for appropriate conformational reorganization. Of course, at higher FBS content, polyplexes bind more proteins/enzymes, which leads to a visible increase in both their mass and size. the Approximately explanation applies the polyplexes in the same to Chit-g-PNIPAM/ADN2000 system, the main difference in this case being that they are already characterized by an initial compact conformation, so that when the FBS components bind, there is a significant increase in their mass and size, especially at a high FBS concentration, where the possibility of secondary aggregation is quite likely.

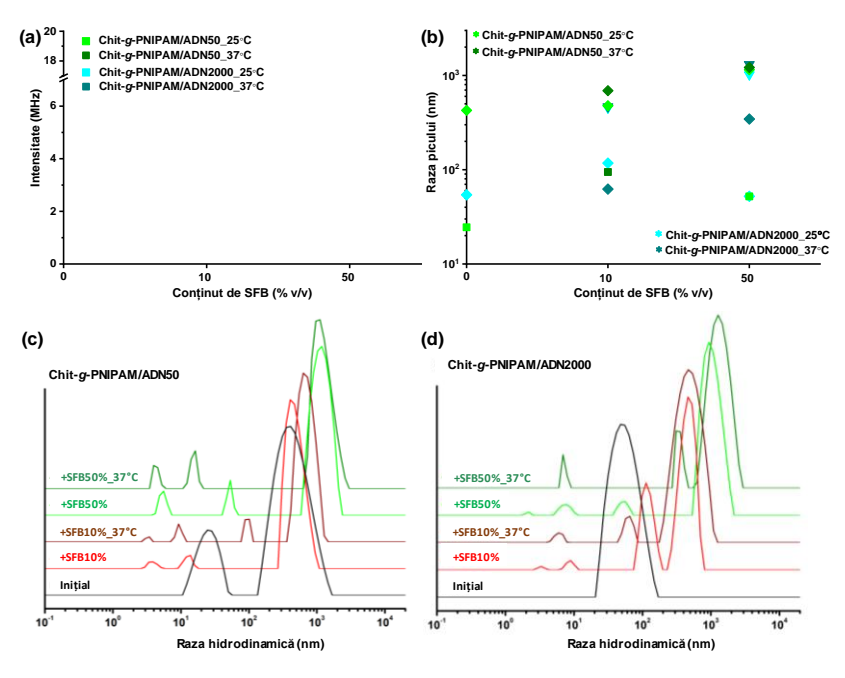


Figure 4.14. Influence of interaction with FBS on (a) scattered light intensity, (b) hydrodynamic radius, (c,d) size distribution functions for polyplexes formed at N/P = 4 in both Chit-g-PNIPAM/ADN50/2000 systems (Karayianni, 2024).

5. Micro- and nanostructured biomaterials based on calcium alginate, in the form of composite hydrogels

5.2. In situ preparation and characterization of ACa-CaCO₃ composite hydrogels

Although the freeze-drying process resulted in well-defined hydrogels, they dissolve rapidly in an aqueous environment. Therefore, the issue of stabilizing the hydrogels for further applications was raised. Since hydrogels are unstable in aqueous solutions, the chosen crosslinking agent was 1% BTCDA solution in acetone, and the morphology of the crosslinked ACa-CaCO₃ hydrogels is shown in Figure 5.5. As can be seen from the SEM images included in Figure 5.5, the porous morphology of the hydrogels was maintained after the cross-linking process, with the pore walls retaining their integrity and orientation. However, the pore size slightly decreased after the washing process (by $\sim 2~\mu m$ in both cases), most likely due to the cross-linking of the polysaccharide chains with BTCDA.

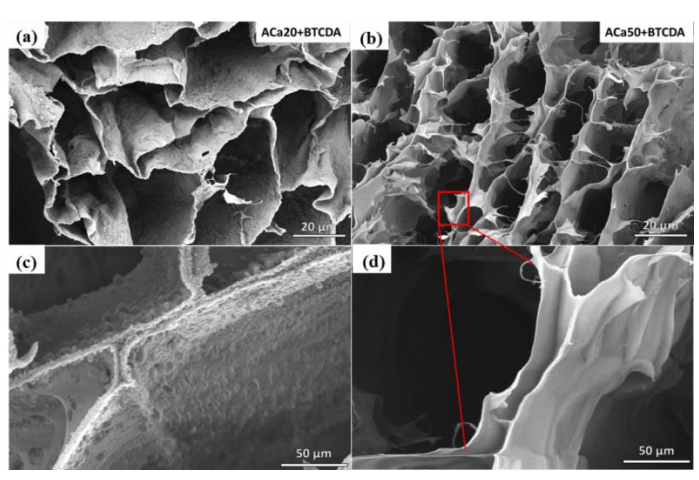


Figure 5.5. SEM images of (a) ACa20-CaCO₃ and (b) ACa50-CaCO₃ after crosslinking with BTCDA; details of the pore wall in ACa50-CaCO₃ (c) before crosslinking and (d) after crosslinking (Mihai, 2024).

During the cross-linking stage, the two anhydride groups of BTCDA can react intraor intermolecularly with the OH groups belonging to the same polymer chain or, respectively, to two polymer chains. The formation of new types of bonds (ester bonds) leads to improved mechanical properties of the material, densifying the organic network. Furthermore, through intensive washing of the samples, excess CaCO₃ crystals were removed from the walls of the hydrogels (this can be seen by comparing the images in Figure 5.4, c and d).

The presence of CaCO₃ in the hydrogel matrix after crosslinking and intensive washing was confirmed by XRD diffractograms (Figure 5.6).

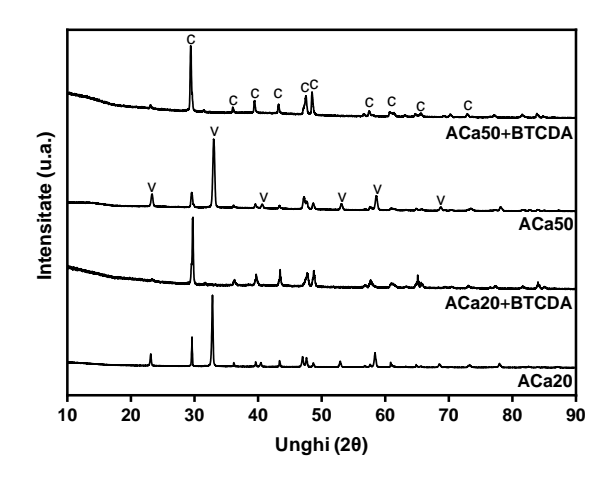


Figure 5.6. XRD diffractograms of ACa20 and ACa50, before and after cross-linking with BTCDA (Mihai, 2024).

As can be seen in Figure 5.6, the uncrosslinked samples (ACa20 and ACa50) have similar diffractograms that highlight the crystalline phases vaterite and calcite. Thus, the presence of vaterite is confirmed by the characteristic intense peak at $2\theta = 33.1$ (114) and the broad peaks at 23.41 (110), 40.68 (211), 53.14 (300), 58.65 (224), and 68.76 (202). The crystallographic planes of calcite, with Miller indices (104), (110), (113), (202), (018), (122), (310), (444), and (431) are represented by diffraction peaks at angles 2θ of 29.41; 35.97; 39.38; 43.26; 47.61; 48.51; 57.40; 61.01; 65.55 and 72.99.

After cross-linking with BTCDA, the characteristic signals of vaterite disappear, while the intensity of all characteristic signals of calcite increases, with the diffractograms showing the most intense peak at $2\theta = 29.4$. This phenomenon can be attributed to the transformation of vaterite into calcite during the cross-linking process through consecutive dissolution-recrystallization processes (Cheng, 2014). Thus, XRD diffractograms demonstrate that, although no CaCO₃ crystals are visible after cross-linking with BTCDA, all hydrogels contain calcite, the most stable polymorph of CaCO₃, confirming the successful *in situ* formation of ACa-CaCO₃ composites, which consist of an alginate matrix reinforced with calcium carbonate nanocrystals.

The MTS assay (Figure 5.8) demonstrated that ACa-CaCO₃ hydrogels have very low cell viability due to the dissolution of the alginate matrix, thus proving the need for a crosslinker to stabilize the hydrogels. After crosslinking with BTCDA and intensive washing of the hydrogels, the materials showed a high increase in relative cell viability after 48 hours in the culture medium, up to 80%. This suggests that ACa-CaCO₃ crosslinked hydrogels may have applications in the biomedical field, having good biocompatibility.

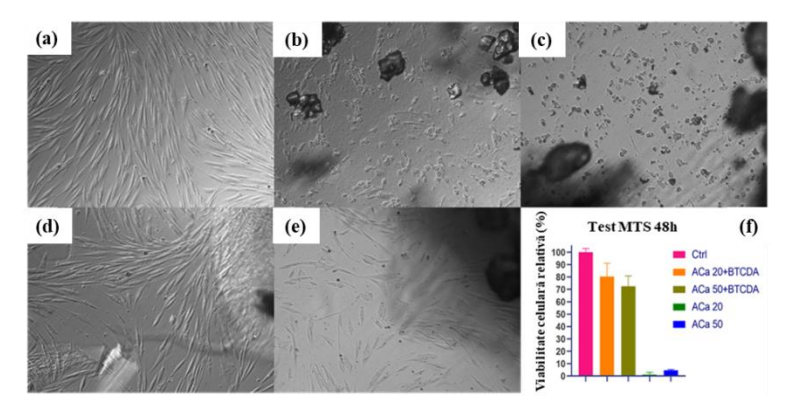


Figure 5.8. Cell morphology after 48 hours of incubation with: (a) control, (b) ACa20, (c) ACa50, (d) ACa20+BTCDA, (e) ACa50+BTCDA; and (f) MTS test results for ACa20 and ACa50 hydrogels, before and after cross-linking (Mihai, 2024).

5.4. Preparation and characterization of multicomponent ACa-CPN-CaCO₃ hydrogels

As can be seen in Figure 5.10, all samples have a hydrogel structure with well-defined pores, both before and after cross-linking. When NPECs with a molar ratio of 0.6 were used, the resulting hydrogels had pores of different sizes, ranging from 3.2 to 15.7 μ m and 2.6 to 12.8 μ m for NPEC Z60/ANa and Z60/CSA, respectively. In the case of NPEC with a molar ratio of 1.2, both samples led to the formation of a more stable network, maintaining the pore walls and their orientation after cross-linking. In addition, the pore size of the hydrogels is more uniform, with an average of 11.2 \pm 2.2 μ m and 8.9 \pm 3.2 μ m when using Z60/ANa 1.2 and Z60/CSA 1.2, respectively. Furthermore, intensive washing of the samples after the cross-linking process did not alter the initial morphology of the hydrogels.

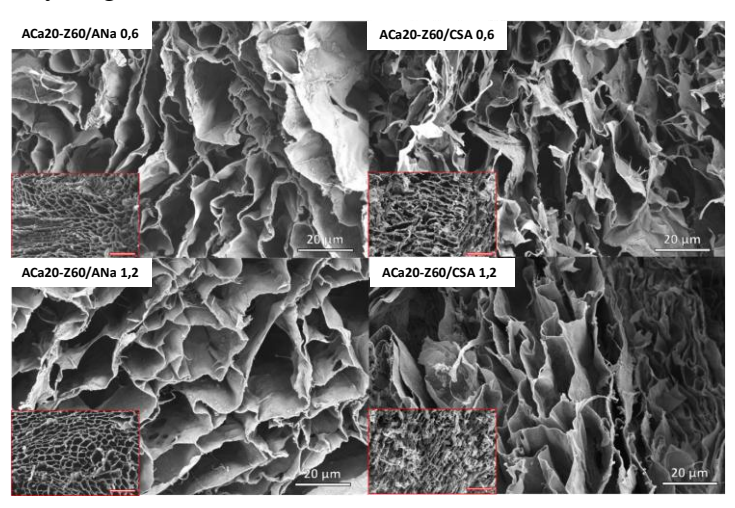


Figure 5.10. SEM images of ACa-CPN-CaCO3 hydrogels after crosslinking with BTCDA; inset SEM images of the corresponding hydrogels before crosslinking with a scale of 100 μm (Mihai, 2024).

Even though all four NPEC dispersions enabled the formation of three-dimensional networks, better organization was achieved when Z60/ANa nanoparticles were used compared to Z60/CSA (Figure 5.10, images of hydrogels before cross-linking); this trend can be correlated with the presence of alginate both in the matrix and on the nanoparticles. As such, the calcium ions present in the reaction medium can interact with the alginate chains in the initial calcium alginate dispersion, as well as with some available sodium alginate chains present on the surface of the nanoparticles, creating "egg-box"-like structures between these two components (Figure 5.2.b), thus increasing the stability of the hydrogels. As shown by SEM images, all hydrogels obtained with NPECs do not show large visible CaCO₃ crystals. The presence of calcium carbonate was highlighted by XRD, the diffractograms obtained for hydrogels being presented in Figure 5.11, in comparison with the diffractograms of the starting materials.

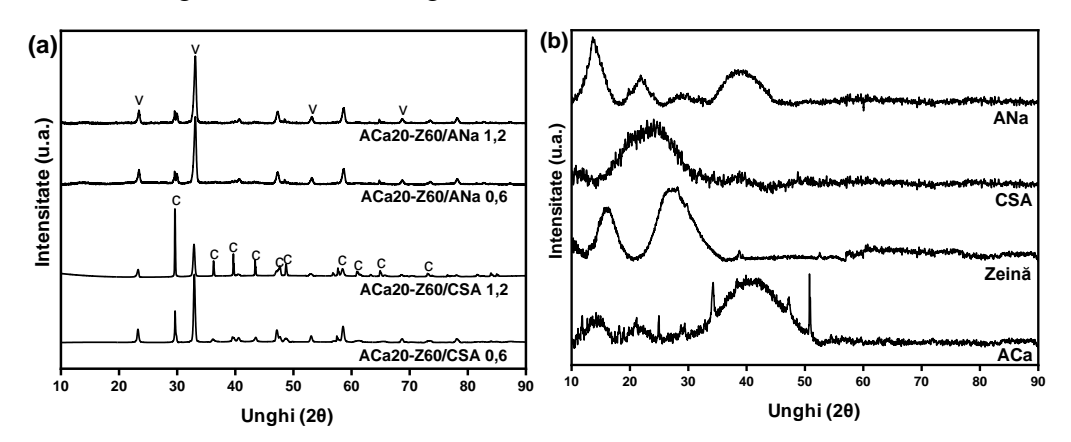


Figure 5.11. XRD diffractograms of (a) ACa-CPN-CaCO₃ hydrogels after crosslinking with BTCDA and (b) ACa used as a matrix for hydrogel and individual CPN components: zein, CSA, and ANa (Mihai, 2024).

The XRD diffractograms demonstrate the presence of $CaCO_3$ in all investigated samples (Figure 5.11a), presenting characteristic peaks for vaterite at $2\theta = 23.30$; 33.1; 56.62; 73.08 and for calcite at $2\theta = 29.61$; 36.25; 39.67 and, respectively, low intensity peaks at 43.41; 47.64; 48.70; 58.43; 61.15; 65.67 and 73.85. The diffractograms of the ACa, zein, CSA, and ANa powders used in these experiments for the preparation of hydrogels are shown in Figure 5.10b. Polysaccharides and zein generally have a broad diffraction band characteristic of their amorphous structure.

The hydrogels obtained with ANa-based NPECs (with both molar ratios) showed fewer and weaker peaks in intensity for calcite, with a percentage of 8.83% in ACa20-Z60/ANa 0.6 and 7.74% in ACa20-Z60/ANa 1.2 (compared to CSA-based CPN (42.9% in ACa20-Z60/CSA 0.6 and 61% in ACa20-Z60/CSA 1.2). These variations can be

attributed mainly to changes in supersaturation conditions within the experiment due to the structure of the polysaccharides used (CSA or ANa).

6. Micro- and nanostructured xanthan-based biomaterials, in the form of oil-in-water emulsions

6.2. Optimization of formulations for the preparation of oil-in-water emulsions

6.2.1. The influence of carrot macerated oil content on the characteristics of oil-inwater emulsions

Carrot macerated oil was selected because it acts as an effective moisturizing ingredient for all skin types, including dry skin. Therefore, formulations with different OC contents (0.5 to 3 mL) were prepared and characterized, and the results of their analysis are included in Figure 6.3.

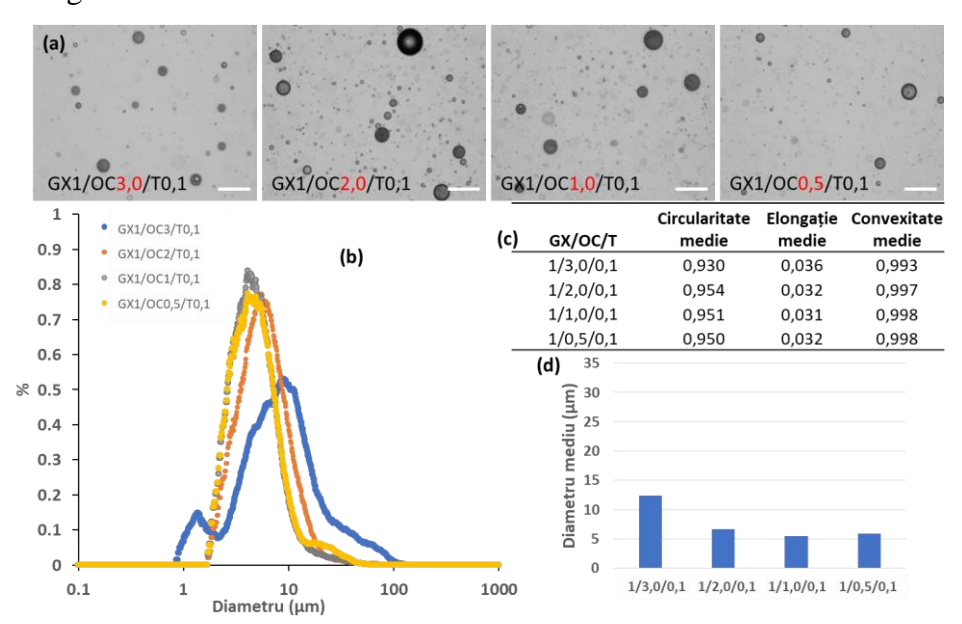


Figure 6.3. Influence of Daucus Carota macerated oil content on O/W emulsion characteristics: (a) images of emulsion droplets (scale = $100 \mu m$), (b) diameter distribution, (c) shape parameters, and (d) mean diameter (Lotos, 2024b).

As can be seen in Figure 6.3 (a, b, and d), regardless of OC content, a relatively wide distribution of droplet sizes was observed, with the average diameter varying slightly as the OC content decreased. However, decreasing the OC content in the formulations reduced the dimensional polydispersity, with the only sample with clear two-dimensional populations being found when the highest OC content was used for the O/W emulsion formulation (GX1/OC3/T0.1). Also, the parameters of circularity (which is a measure of the approximation to a perfect circle) and convexity (a measure of the roughness of a particle's surface), very close to the value of one, together with an elongation (a measure of

the length/width ratio) close to zero, confirm the spherical shape of the droplets, regardless of the OC content, as can be seen in Figure 6.3c.

6.3. Study of the biological properties of oil-in-water emulsions

6.3.1. The cytotoxic behavior of oil-in-water emulsions

The cytotoxicity of normal human fibroblast cells (NHDF) after 24 hours of contact with the tested samples was compared with that of untreated cells, with the results shown in Figure 6.10. According to ISO 10993-5:2009, a reduction in cell viability of more than 30% is considered a cytotoxic effect. Thus, as shown in Figure 6.10, after 24 hours of treatment, it appears that emulsions with a lower surfactant content (GX1/OC3/T0.1, GX1/OC1/T0.1, and GX1/OC2/T0.1) are not cytotoxic, regardless of OC content. On the other hand, the sample with the highest surfactant content (GX1/OC3/T3) proved to be cytotoxic to NHDF cells, most likely due to the high amount of surfactant, as Tween 80 is known to have a cytotoxic effect on normal human fibroblasts (Arechabala, 1999).

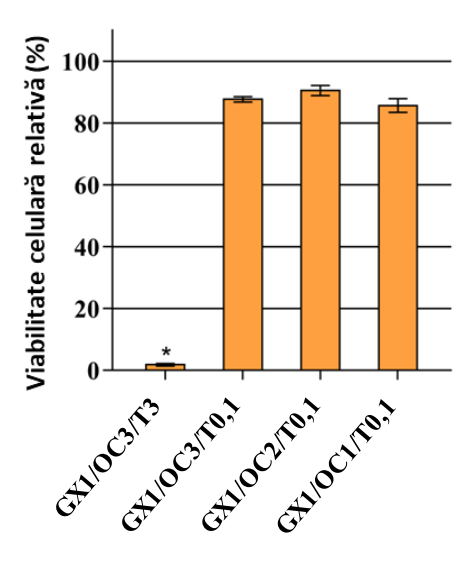


Figure 6.10. Cytotoxicity of NHDF cells treated for 24 hours with O/W emulsions, compared to untreated cells. Results are presented as mean \pm standard error of the mean, n=3; *p<0.05 (Lotos, 2024b).

6.3.2. Antimicrobial activity of oil-in-water emulsions

Antimicrobial activity was evaluated against four different microorganisms (*E. coli*, *K. pneumoniae*, *E. faecalis*, and *C. glabrata*) using the Kirby-Bauer test, known as the disc diffusion method, with the diameters of the inhibition zones shown in Table 6.1, together with the minimum inhibitory concentrations (MIC) determined by the dilution method in culture medium.

Table 6.1. Antimicrobial activity of O/W emulsions against reference strains: results of the disc diffusion method and minimum inhibitory concentration, MIC (Lotos, 2024b).

Emulsion	GX1/OC3/T3	GX1/OC3/T0.1	GX1/OC2/T0.1	GX1/OC1/T0.1	
Strains	Inhibition zone (mm)				
E. coli	10.30 ± 0.28	11.85 ± 0.21	11.55 ± 0.77	12.00 ± 0.28	
K. pneumoniae	8.20 ± 0.14	9.20 ± 0.14	9.25 ± 0.21	8.65 ± 0.49	
E.faecalis	10.30 ± 0.56	12.10 ± 0.14	11.80 ± 0.42	12.55 ± 0.35	
C.glabrata	13.30 ± 0.99	13.25 ± 0.77	13.15 ± 0.48	14.15 ± 0.48	
	MIC (mg/mL)				
E. coli	49.69	52.46	35.65	18.18	
K. pneumoniae	49.69	52.46	35.65	18.18	
E.faecalis	49.69	52.46	35.65	18.18	
C.glabrata	49.69	52.46	35.65	18.18	

All samples were effective against the bacterial strains *E. coli*, *K. pneumoniae*, *E. faecalis*, and the best results were obtained in the case of yeasts represented by *C. glabrata* (approximately 14 mm inhibition zone for each sample tested). Sample GX1/OC1/T0.1 had the best antimicrobial activity, with the lowest inhibitory concentration (18.18 mg/mL) and the best antimicrobial results. However, the estimation of antimicrobial activity shows that there were no notable differences between the tested samples, and the presence of surfactant does not influence the antimicrobial activity of the samples of their concentration. The explanation is that the antimicrobial activity of the samples is due to *Daucus carota* oil, already used for some skin conditions such as burns and furunculous (Glišić, 2007). Similar antifungal properties have previously been reported in the literature against *C. albicans* (Alves-Silva, 2016; Marzouki, 2010), but also against *E. coli* (Soković, 2009).

6.5. Preparation of textile supports treated with oil-in-water emulsions and their evaluation as cosmetic textiles

6.5.1. Analysis of comfort indices

Comfort indices are essential for cosmetic textiles, as they play a key role in determining the comfort and performance of these products. The values obtained for air permeability, hygroscopicity, and water vapor permeability are shown in Table 6.2.

Table 6.2. Comfort indices for textiles treated with emulsions (Lotos, 2024b).

Sample	Air permeability	Hygroscopicity	Vapor permeability
Control sample	19.2388±0.06	1.9420±0.009	18.6836±0.04
GX1/OC3/T0.1	16.0944 ± 0.06	9.7627 ± 0.02	17.6928 ± 0.02
GX1/OC2/T0.1	17.0833 ± 0.08	6.9306 ± 0.01	17.8343 ± 0.02
GX1/OC1/T0.1	17.4166 ± 0.08	7.4468 ± 0.01	18.0467±0.04

According to the results presented in Table 6.2, air permeability decreased compared to the control sample. One possible explanation is that the emulsions filled the spaces between the fibers, making the textile surface denser (as can be seen in the inserts in Figure 6.12). Thus, the textile support treated with the emulsion containing the lowest amount of macerated *Daucus Carota* oil has the highest permeability value (sample treated with emulsion GX1/OC1/T0.1), and the sample containing the highest amount of oil has the lowest value (samples treated with the GX1/OC3/T0.1 emulsion). On the other hand, the decrease in air permeability is not so significant as to affect the breathability and comfort of the textile substrates.

The results obtained show that the hygroscopicity values for textile substrates treated with emulsions are higher than the hygroscopicity of the control sample, suggesting that the treated textiles are capable of absorbing more moisture from the skin. One possible explanation may be that the fatty acids in the composition of macerated *Daucus Carota* oil and the polysaccharide may act as potential hygroscopic agents (Sumathi, 2007). On the other hand, increased hygroscopicity leads to a decrease in air and water permeability due to the swelling and closure of pores in textile substrates (Kapoor, 2021).

Textiles treated with emulsions have lower water vapor permeability than the control sample. One possible explanation is that applying the emulsion may block some of the pores in the textile substrate. However, the decrease in water vapor permeability of samples treated with emulsions is not so significant as to influence temperature regulation and perspiration.

6.5.2. Assessment of skin hydration through the application of functionalized textiles with oil-in-water emulsions

The textiles treated with emulsions were further studied to determine the degree of skin hydration, being applied to different areas on the inner side of the forearms. The degree of skin hydration was measured immediately after removing the textiles treated with emulsions from the skin (after 1 hour) and 24 hours after applying the functional textiles to the skin, with the results presented by age group in Figure 6.13.

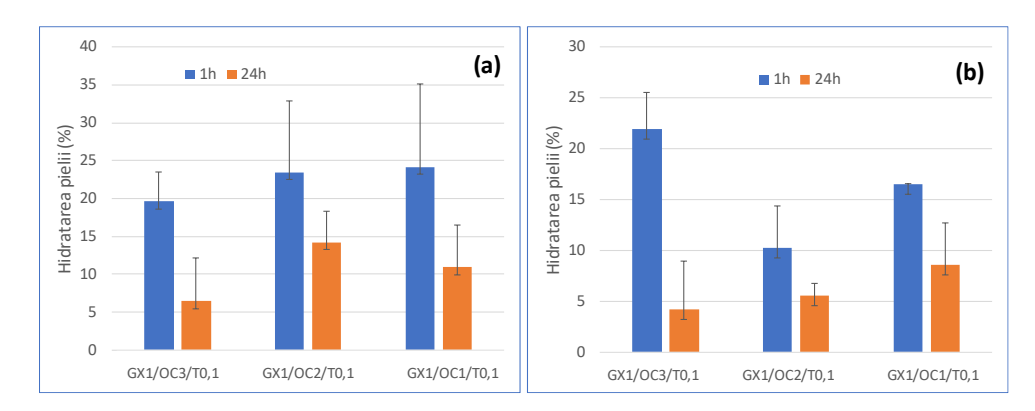


Figure 6.13. Variation in skin hydration levels for the age groups (a) 31–40 years and (b) >65 years (Lotos, 2024b).

According to the results obtained, skin hydration values when applying textile supports treated with emulsions are higher than those obtained by simply applying emulsions to the skin (Figure 6.13a and b). One possible explanation is that applying the emulsion-treated textile to the skin creates an occlusive barrier that helps retain moisture and prevents water loss from the skin surface (Harwood, 2024), and thus emulsion-treated textiles lead to greater skin hydration. On the other hand, even though emulsions applied directly to the skin are absorbed very easily, due to the lack of a barrier to retain moisture, they evaporate more quickly and thus reduce skin hydration over time.

GENERAL CONCLUSIONS

The doctoral thesis entitled "Micro- and nanostructured biomaterials based on polysaccharides: preparation, structure, and properties" had as its general objective the preparation of new micro- and nanostructured biomaterials based on polysaccharides and other natural or synthetic polymers and the characterization of their structure and properties. The work spans 196 pages and comprises six chapters that include 128 figures, 17 tables, 11 equations, one diagram, and 307 bibliographic references. The doctoral thesis is structured in two parts: the current state of knowledge and original results structured in five chapters.

To achieve the main objective of the thesis, three directions of study were followed:

- 1. Micro- and nanostructured biomaterials based on polysaccharides, in the form of interpolymeric complexes and polyplexes
 - preparation and characterization of non-stoichiometric interpolymeric complexes based on polysaccharides and other natural polymers
 - preparation and characterization of interpolymeric complexes based on polysaccharides and synthetic polymers

- preparation and characterization of Chit-g-PNIPAM and DNA-based polyplexes

2. Micro- and nanostructured biomaterials based on calcium alginate, in the form of composite hydrogels

- *in situ* preparation and characterization of calcium alginate-CaCO₃ composite hydrogels
- preparation and characterization of multicomponent calcium alginate-NPEC-CaCO₃ hydrogels

3. Micro- and nanostructured xanthan-based biomaterials, in the form of oil-in-water emulsions

- preparation of oil-in-water emulsions using xanthan gum and macerated oil from *Daucus Carota* and study of biological properties
- preparation of textile supports treated with oil-in-water emulsions and their evaluation as cosmetic textiles

Based on the original studies conducted as part of the doctoral thesis, the following conclusions can be drawn:

1. Preparation and characterization of non-stoichiometric interpolymeric complexes based on polysaccharides and other natural polymers:

- the first part of Chapter 3 of the thesis contains original results regarding the preparation and characterization of NPECs containing zein and two types of polysaccharides (CSA and ANa);
- the behavior of zein at different alcohol-water concentrations and different pH values was evaluated to establish the optimal conditions for complex formation;
- NPECs were synthesized using two *complementary addition methods* (the titrant was either zein or polysaccharide) and at two different addition rates (0.3 and 0.8 ml/min), with a molar ratio between complementary loads ranging from 0.4 to 1.8;
- when zein was the titrant, particles with large sizes and high polydispersity were obtained;
- when zein was the titrant and at molar ratios below 1.2, *particles with an average* size of approximately 100 nm were obtained, which were almost monodisperse; when polysaccharides were the titrated macromolecules, they were able to easily incorporate zein, forming core/shell structures;

- a change in the content of α-helical secondary elements of zein was observed depending on its content in NPECs, with polysaccharide binding most likely destroying the hydrogen bond between the polypeptide chains of zein, leading to a decrease in the helical structure fraction;
- NPEC dispersions with the best characteristics (molar ratio between polymers of 0.8, size of 100 nm, zeta potential of -20 mV) were successfully used to encapsulate ciprofloxacin with the *formation of three-component complexes*;
- The antibacterial activity of CF/NPEC was evaluated against S. aureus and E. coli by treating a nonwoven cellulose material with the three-component complex dispersion, and it was demonstrated that the drug retains its antibacterial activity, which is more pronounced in the case of E. coli.

2. Preparation and characterization of interpolymeric complexes based on polysaccharides and synthetic polymers:

- the second part of Chapter 3 presents the preparation of natural-synthetic macromolecular nanostructures formed by the electrostatic interaction of chitosan polysaccharide molecules and PNIPAM samples functionalized at one end with a carboxylate group, as an alternative method of grafting polysaccharides with synthetic polymer chains;
- various combinations of long or short chains of both macromolecular components were studied at different mixing ratios, and stable complexes were obtained;
- their physicochemical properties in terms of mass, size, charge, structure, and morphology were examined by DLS, potentiometry, fluorescence spectroscopy, as well as STEM and AFM imaging;
- it was found that the individual characteristics of the complexes formed are directly correlated with the length of the chitosan and PNIPAM molecules (long/short) and with their mixing ratio;
- the influence of the length of the chitosan molecule proved to be particularly significant, as it led to the formation of complexes with a different arrangement of components and a different structure, either relaxed or dense;
- Chit/PNIPAM complexes exhibit similar temperature-dependent behavior due to the thermosensitive nature of PNIPAM chains, showing conformational

- changes when the temperature rises above 35 °C, which are completely reversible when the temperature drops to room temperature;
- Chit/PNIPAM complexes are sensitive to variations in the ionic strength of the solution, exhibiting a reduction or partial disassembly (depending on their initial conformation) as a result of charge screening;
- the potential use of these nanostructures as delivery vectors for bioactive molecules was verified by successfully encapsulating curcumin, as a result of the hydrophobic interactions that occur between the bioactive molecule and the complexes, and the results obtained highlight the importance of the balance between electrostatic and hydrophobic interactions when it comes to such structurally complex systems.

3. Preparation and characterization of chitosan-g-poly(N-isopropylacrylamide) copolymer:

- in the first part of Chapter 4, the thermosensitive copolymer Chit-g-PNIPAM was successfully obtained by the "grafting onto" chitosan method through the covalent bonding of PNIPAM chains, a synthetic polymer obtained by RAFT polymerization;
- the formation of the Chit-*g*-PNIPAM copolymer was demonstrated by FTIR-ATR and ¹H-NMR spectroscopy, TGA, and reverse conductometric titrations;
- grafting efficiency was quantified as 19.9% by ¹H-NMR and 21.62% by conductometric titration;
- the Chit-g-PNIPAM copolymer exhibited thermosensitive self-assembly in aqueous solutions, as evidenced by light scattering measurements as a function of temperature (temperature range 25–45 °C);
- the Chit-g-PNIPAM copolymer, with its thermosensitive properties, can be
 used in the development of new smart nanocontainers for the transport and
 delivery of nucleic acids.

4. Preparation and characterization of Chit-g-PNIPAM and DNA-based polyplexes:

 the second part of Chapter 4 presents an experimental study focused on the interaction between the Chit-g-PNIPAM copolymer and two DNA molecules of different lengths, as well as on the physicochemical properties of the formed polyplexes;

- the general physicochemical characteristics of the polyplexes in terms of their mass, size, charge, structure, and stability proved to be a complex combination of the ratio between the two macromolecular components, the length of the DNA molecule, and the intrinsic conformation of the Chit-g-PNIPAM copolymer;
- the presence of PNIPAM side chains gives the polyplexes thermosensitive behavior, thus enabling additional functionality with fully reversible conformational changes of the already formed polyplexes, which occur at an LCST of 35 °C;
- the stability of the polyplexes was also examined when the ionic strength was increased or when they interacted with biological fluids such as FBS, and it was found that they are extremely resistant to both destabilizing factors;
- the binding affinity between the copolymer and DNA chains was monitored by
 quenching the fluorescence of samples marked with ethidium bromide, and it
 was demonstrated that this is greatly influenced by the length of the DNA
 molecule, in the sense that shorter chains are easier to complex due to their
 conformation and, therefore, easier to incorporate into the formed polyplexes;
- FTIR spectra showed that Chit-*g*-PNIPAM protects the native conformation of both short and long DNA molecules;
- the study highlighted the complexity of such systems and how they can be characterized from a physicochemical point of view, while also highlighting the number of parameters that must be taken into account when designing potential gene delivery systems for biological applications.

5. Preparation and characterization of micro- and nanostructured biomaterials based on calcium alginate, in the form of composite hydrogels:

- Chapter 5 demonstrates the successful preparation of composite hydrogels with calcium carbonate, starting from ACa, using the ammonium carbonate diffusion method and *in situ* crystallization of CaCO₃;
- the ACa concentration varied from 2 to 50 g/L, with the best porous structure being obtained when a higher concentration was used;
- the stabilization of the formed hydrogels was achieved with the BTCDA crosslinker, with MTS tests showing that the crosslinked hydrogels have a relative cell viability of up to 80% after 48 hours;

- the second stage of the study on composite hydrogel formulations used, in addition to the materials used in the first stage, NPECs based on zein and the polysaccharides ANa and CSA (whose synthesis and characterization are described in detail in Chapter 3, Part I);
- the resulting hydrogels showed good three-dimensional organization, without excess large CaCO₃ crystals, demonstrating good stability during the cross-linking process.

6. Preparation and characterization of micro- and nanostructured xanthan-based biomaterials, in the form of oil-in-water emulsions:

- in Chapter 6, ten O/W emulsions were obtained and characterized by a series of specific analyses (organoleptic properties, dimensional analysis, turbidity, surface tension of droplets and contact angle, pH, and electrical conductivity);
- both OC and GX play an important role in the properties of the O/W emulsion, the best formulation conditions (in terms of stability and subsequent topical application) being: GX 1% wt. in the initial solution, surfactant (T) 0.1 mL, regardless of the amount of OC used;
- *in vivo* tests have shown that O/W emulsions with macerated *Daucus Carota* oil can effectively improve the overall level of skin hydration, leaving it soft and smooth;
- the biocompatible emulsions were applied to knitted cellulose fabrics, and the resulting skin care textiles exhibit good comfort properties and a higher degree of skin hydration compared to emulsions applied directly to the skin;
- applying emulsions to textile substrates to create textiles with moisturizing properties is an original and unconventional approach; applying such technologies can have a positive impact on sustainability by reducing the need for synthetic materials or chemical treatments.

The conducted studies identified some research **perspectives** that could be developed in the future, such as:

- the use of polyelectrolyte complexes based on polysaccharides and other natural or synthetic polymers for the encapsulation and release of drugs with antibacterial effects, such as doxycycline or minocycline;
- optimization of the PNIPAM grafting process on chitosan to achieve controlled grafting efficiency and, therefore, improved properties;

- incorporation of drugs or antibiotics into the matrix of ACa-CPN-CaCO₃ composite hydrogels and testing of their properties;
- using other active ingredients to produce functional textiles with improved skin care properties;
- testing the materials obtained for subsequent use in environmental applications, as sorbents for various pollutants.

The dissemination of the original results presented in this doctoral thesis was achieved through the publication of six scientific articles in ISI-rated journals (with a cumulative impact factor of 27.2), three of which were as first author. The results presented are also supported by seven oral presentations and five poster presentations at national and international conferences, supplemented by one scientific article, three oral presentations, and one poster presentation, the results of which are not presented in the thesis. The results obtained were made possible thanks to the financial support of three national research projects and by completing two research internships and participating in a summer school.

SELECTIVE REFERENCES

Alves, N.M., Mano, J.F., 2008. Chitosan derivatives obtained by chemical modifications for biomedical and environmental applications. *Int. J. Biol. Macromol.* 43, pp.401–414.

Alves-Silva, J.M., Zuzarte, M., Gonçalves, M.J., Cavaleiro, C., Cruz, M.T., Cardoso, S.M., Salgueiro, L., 2016. New claims for wild carrot (*Daucus carota* subsp. *carota*) essential oil. *Evid. Based Complement Alternat. Med.* 2016(1), p.9045196.

Arechabala, B., Coiffard, C., Rivalland, P., Coiffard, L.J.M., Roeck-Holtzhauer, Y.D., 1999. Comparison of cytotoxicity of various surfactants tested on normal human fibroblast cultures using the neutral red test, MTT assay and LDH release. *J. Appl Toxicol.* 19(3), pp.163-165.

Bao, H., Li, L., Leong, W.C., Gan, L.H., 2010. Thermo-responsive association of chitosan-*graft*-poly(*N*-isopropylacrylamide) in aqueous solutions. *J. Phys. Chem. B* 114, pp.10666–10673.

Campoli-Richards, D.M., Monk, J.P., Price, A., Benfield, P., Todd, P.A., Ward, A., 1988. Ciprofloxacin. A review of its antibacterial activity, pharmacokinetic properties and therapeutic use. *Drugs* 35(4), pp.373-447.

Chalanqui, M., Pentlavalli, S., McCrudden, C., Chambers, P., Ziminska, M., Dunne, N., McCarthy, H., 2019. Influence of alginate backbone on efficacy of thermo-responsive alginate-*g*-P(NIPAAm) hydrogel as a vehicle for sustained and controlled gene delivery. *Mater. Sci. Eng. C* 95, pp.409–421.

Cheaburu-Ylmaz, C.N., 2020. On the Development of chitosan-*graft*-poly(*N*-isopropylacrylamide) by raft polymerization technique. *Cellul. Chem. Technol.* 54, pp.1–10.

Fathi, M., Alami-Milani, M., Geranmayeh, M.H., Barar, J., Erfan-Niya, H., Omidi, Y., 2019. Dual thermo-and pH-sensitive injectable hydrogels of chitosan/(poly(*N*-isopropylacrylamide-*co*-itaconic acid)) for doxorubicin delivery in breast cancer. *Int. J. Biol. Macromol.* 128, pp.957–964.

Glišić, S.B., Mišić, D.R., Stamenić, M.D., Zizovic, I.T., Ašanin, R.M., Skala, D.U., 2007. Supercritical carbon dioxide extraction of carrot fruit essential oil: Chemical composition and antimicrobial activity. *Food chem.* 105(1), pp.346-352.

Harwood, A., Nassereddin, A., Krishnamurthy, K., 2024. Moisturizers. În: *StatPearls* [*Internet*]. StatPearls Publishing.

Kapoor, A., Baronia, A.K., Azim, A., Agarwal, G., Prasad, N., Mishra, R., Saraswat, V.A., 2021. Breathability and safety testing of personal protective equipment: "Human-comfort" factor remains undefined. *Indian J. Crit. Care Med.* 25(1), p.12.

Karayianni, M., **Lotos, E.D.**, Mihai, M., Pispas, S., 2024. Coassembly of a Hybrid Synthetic–Biological Chitosan-*g*-Poly(*N*-isopropylacrylamide) Copolymer with DNAs of Different Lengths. *Polymers* 16(21), p.3101.

Kumar, S., Koh, J., 2012. Physiochemical, optical and biological activity of chitosan-chromone derivative for biomedical applications. *Int. J. Mol. Sci.* 13, pp.6102–6116.

- Li, G., Zhuang, Y., Mu, Q., Wang, M., Fang, Y., 2008. Preparation, characterization and aggregation behavior of amphiphilic chitosan derivative having poly(L-lactic acid) side chains. *Carbohydr. Polym.* 72, pp.60–66.
- **Lotos, E.D.**, Danila, A., Vasiliu, A.L., Rosca, I., Stroian, D.V., Simionescu, B.C., Mihai, M., 2024b. The potential emulsions of xanthan gum and *Daucus carota* macerated oil in functional textiles for skincare applications: Formulation, characterization, and performance evaluation. *Colloids Surf.*, A 682, p.132960.
- **Lotos, E.D.**, Karayianni, M., Vasiliu, A.L., Mihai, M., Pispas, S., 2025. Natural—Synthetic Hybrid Nanostructures Formed Through the Interaction of Chitosan with Carboxylate-Ended PNIPAM: Structure and Curcumin Encapsulation. *Nanomaterials* 15(5), p.350.
- **Lotos, E.D.**, Mihai, M., Vasiliu, A.L., Rosca, I., Mija, A., Simionescu, B.C., Pispas, S., 2024a. Zein/polysaccharide nanoscale electrostatic complexes: preparation, drug encapsulation and antibacterial properties. *Nanomaterials* 14(2), p.197.
- Marzouki, H., Khaldi, A., Falconieri, D., Piras, A., Marongiu, B., Molicotti, P., Zanetti, S., 2010. Essential oils of *Daucus carota* subsp. *carota* of Tunisia obtained by supercritical carbon dioxide extraction. *Nat. Prod. Commun.* 5(12), p.1934578X1000501226.
- Mihai, M., Lotos, E.D., Zaharia, M.M., Bucatariu, F., Vasiliu, A.L., 2024. Alginate-based Composite Hydrogels Formed by *In Situ* CaCO₃ Crystallization. *Cryst. Growth Des.* 24(6), pp.2514-2525.
- Queiroz, M., Melo, K.R.T., Sabry, D.A., Sassaki, G.L., Rocha, H.A.O., 2014. Does the use of chitosan contribute to oxalate kidney stone formation? *Mar. Drugs* 13, pp.141-158.
- Soković, M., Stojković, D., Glamočlija, J., Ćirić, A., Ristić, M., Grubišić, D., 2009. Susceptibility of pathogenic bacteria and fungi to essential oils of wild *Daucus carota*. *Pharm Biol.* 47(1), pp.38-43.
- Sosnik, A., Imperiale, J.C., Vázquez-González, B., Raskin, M.M., Muñoz-Muñoz, F., Burillo, G., Cedillo, G., Bucio, E., 2015. Mucoadhesive thermo-responsive chitosan-*g*-poly(*N*-isopropylacrylamide) polymeric micelles *via* a one-pot gamma-radiation-assisted pathway. *Colloids Surf.*, *B* 136, pp.900–907.
- Sumathi, A., Ushakumari, S.R., Malleshi, N.G., 2007. Physico-chemical characteristics, nutritional quality and shelf-life of pearl millet based extrusion cooked supplementary foods. *Int. J. Food Sci. Nutr.* 58(5), pp.350-362.
- Vasiliu, A.-L., Zaharia, M.-M., Bazarghideanu, M.-M., Rosca, I., Peptanariu, D., Mihai, M., 2022. Hydrophobic composites designed by a nonwoven cellulose-based material and polymer/CaCO₃ patterns with biomedical application. *Biomacromolecules* 23(1), pp.89–99.
- Wang, W., Yu, W., 2015. Preparation and characterization of CS-g-PNIPAAm microgels and application in water vapor-permeable fabric. *Carbohydr. Polym.* 127, pp.11–18.
- Zaharia, M.-M., Bucatariu, F., Karayianni, M., **Lotos, E.-D.**, Mihai, M., Pispas, S., 2024. Synthesis of Thermoresponsive Chitosan-*Graft*-Poly(*N*-Isopropylacrylamide) Hybrid Copolymer and Its Complexation with DNA. *Polymers 16*, p.1315.

DISSEMINATION OF RESULTS OBTAINED DURING THE DOCTORAL STUDIES

Scientific papers published in ISI-rated scientific journals (results included in the thesis):

- 1. **E.-D. Lotos**, M. Mihai, A.-L. Vasiliu, I. Rosca, A. Mija, B. C. Simionescu, S. Pispas; Zein/polysaccharides nanoscale electrostatic complexes: preparation, drug encapsulation and antibacterial properties; *Nanomaterials* 14(2), 197, **2024** (IF₂₀₂₄ = 4.3). DOI: 10.3390/nano14020197
- 2. **E.-D. Lotos**, A. Danila, A.-L. Vasiliu, I. Rosca, D.-V. Stroian, B. C. Simionescu, M. Mihai; The potential emulsions of xanthan gum and *Daucus carota* macerated oil in functional textiles for skincare applications: Formulation, characterization, and performance evaluation; *Colloids and Surfaces A: Physicochemical and Engineering Aspects* 682, 132960, **2024** (IF₂₀₂₄ = 5.4). DOI: 10.1016/j.colsurfa.2023.132960
- 3. M. Mihai, E.-D. Lotos, M.-M. Zaharia, F. Bucatariu, A.-L. Vasiliu; Alginate-based composite hydrogels formed by *in-situ* CaCO₃ crystallization; *Crystal Growth & Design* 24(6), 2514-2525, **2024** (IF₂₀₂₄ = 3.4). DOI: 10.1021/acs.cgd.3c01518
- 4. M.-M. Zaharia, F. Bucatariu, M. Karayianni, **E.-D. Lotos**, M. Mihai, S. Pispas; Synthesis of thermoresponsive chitosan-*graft*-poly(*N*-isopropylacrylamide) hybrid copolymer and its complexation with DNA; *Polymers* 16(10), 1315, **2024** (IF₂₀₂₄ = 4.9). DOI: 10.3390/polym16101315
- 5. M. Karayianni, **E.-D. Lotos**, M. Mihai, S. Pispas; Coassembly of a hybrid synthetic—biological chitosan-*g*-poly(*N*-isopropylacrylamide) copolymer with DNAs of different lengths; *Polymers* 16(21), 3101, **2024** (IF₂₀₂₄ = 4.9). DOI: 10.3390/polym16213101
- 6. **E.-D. Lotos**, M. Karayianni, A.-L. Vasiliu, M. Mihai, S. Pispas; Natural—synthetic hybrid nanostructures formed through the interaction of chitosan with carboxylate-ended PNIPAM: Structure and curcumin encapsulation; *Nanomaterials* 15(5), 350, **2025** (IF₂₀₂₄ = 4.3). DOI: 10.3390/nano15050350

Scientific papers published in ISI-rated scientific journals (results not included in the thesis):

1. **E.-D. Lotos**, R. Dinu, M. Mihai, B. C. Simionescu, A. Mija; Development of Eco-Friendly Thermosetting Resins From Zein and Diglycidyl Ether of Vanillyl Alcohol. A Step Toward Sustainable Materials; *Chemistry - A European Journal* 31(27), e202500624, **2025** (IF₂₀₂₄ = 3.7). DOI: 10.1002/chem.202500624

Scientific papers published *in extenso* in the proceedings of scientific events:

1. M. Karayianni, **E.-D. Lotos**, A.-L. Vasiliu, M. Mihai, S. Pispas; Hybrid nanostructures of chitosan and poly(*N*-isopropylacrylamide) with carboxylate end group; Proceedings of International Conference Progress in Organic Macromolecular Compounds, ISSN 2810–2347 ISSN–L 2810–2126, 47-50, **2023**.

- E.-D. Lotos, A.-L. Vasiliu, M. Mihai, B.C. Simionescu; Nonstoichiometric polyelectrolyte complex nanoparticles based on zein and polysaccharides; Proceedings of International Conference Progress in Organic Macromolecular Compounds, ISSN 2810–2347 ISSN–L 2810–2126, 92-95, 2023.
- 3. A.-L. Vasiliu, **E.-D. Lotos**, M.-M. Zaharia, M. Mihai; Composite hydrogels based on alginates and calcium carbonate; Proceedings of International Conference Progress in Organic Macromolecular Compounds, ISSN 2810–2347 ISSN–L 2810–2126, 77-80, **2023**.
- 4. **E.-D. Lotos**, M. Karayianni, M. Mihai, S. Pispas; New polysaccharide grafting method pairing Chitosan with PNIPAM bearing carboxyl end group; Proceedings of International Conference Progress in Organic Macromolecular Compounds, ISSN 2810–2126 ISSN–L 2810–2126, 148-150, **2025**.
- M. Karayianni, E.-D. Lotos, M. Mihai, S. Pispas; Chitosan-g-Poly(*N*-isopropylacrylamide) polyplexes with DNA molecules of different lengths; Proceedings of International Conference Progress in Organic Macromolecular Compounds, ISSN 2810–2126 ISSN–L 2810–2126, 136-138, 2025.

Oral presentations at national and international scientific events (results included in the thesis):

- 1. E.-D. Lotos, A.-L. Vasiliu, B. C. Simionescu, M. Mihai; Composite particles based on zein and polysaccharides; 20th National Symposium Polymers 2022 open to International Participation (POLYMERS 2022), 5–8 July 2022, Velingrad, Bulgaria.
- 2. **E.-D. Lotos**, A.-L. Vasiliu, M. Mihai, B. C. Simionescu; Composite nanoparticles based on zein and polysaccharides; *NeXT-Chem V: Exploratory Workshop "Innovative cross-sectoral technologies"*, 22–23 May **2023**, Bucharest, Romania.
- 3. **E.-D. Lotos**, M. Mihai, A.-L. Vasiliu, B. C. Simionescu; Zein/polysaccharide nanoparticles as drug delivery systems; *29th PolyChar World forum on Advanced Materials*, 25–29 September **2023**, Nice, France.
- E.-D. Lotos, M. Karayianni, A.-L. Vasiliu, L.-M. Petrila, M. Mihai, S. Pispas, B. C. Simionescu; Interaction between water-soluble chitosan and thermo-responsive poly(*N*-isopropylacrylamide); *ICMPP Open door to the future scientific communications of young researchers* 4th edition (MacroYouth 2023), 17 November 2023, Iasi, Romania.
- E.-D. Lotos, M. Karayianni, A.-L. Vasiliu, B. C. Simionescu, S. Pispas, M. Mihai; Thermo-responsive hybrid nanostructures of chitosan and poly(*N*-isopropylacrylamide); 6th Edition, Innovation trans-sectorial technology (NeXT-Chem 2024), 21–22 March 2024, Bucharest, Romania.
- 6. **E.-D. Lotos**, A. Danila, M. Mihai, B. C. Simionescu; Xanthan gum-based emulsions in functional textiles for skincare applications; 7th International Conference of the Doctoral School, 15–17 May **2024**, Iasi, Romania.
- 7. M. Karayianni, **E.-D. Lotos**, M. Mihai, S. Pispas; Effect of DNA length on the formation of novel chitosan-*graft*-poly(*N*-isopropylacrylamide) based polyplexes;

EPF European Polymer Congress (EPF 2025), 22-27 June 2025, Groningen, Netherlands.

Poster presentations at national and international scientific events (results included in the thesis):

- 1. **E.-D. Lotos**, M. Karayianni, A.-L. Vasiliu, B. C. Simionescu, S. Pispas, M. Mihai; Hybrid polysaccharides-based nanostructures with thermo-responsive behaviour; *NATO ASI Summer School*, 28 June–5 July **2024**, Smolenice, Slovak Republic.
- 2. **E.-D. Lotos**, M. Karayianni, M. Mihai, S. Pispas; Co-assembly of Chitosan-g-Poly(N-isopropylacrylamide) copolymer with DNAs; 5th Edition OPEN DOOR TO THE FUTURE Scientific Communications of Young Researchers with international participation (MacroYouth 2024), 15 November **2024**, Iasi, Romania.
- 3. C.-G. Marandiş, M.-M. Zaharia, L.-M. Petrila, **E.-D. Lotos**, F. Bucatariu, I. Mangalagiu, M. Mihai, S. Pispas; Chit-*g*-PNIPAM: A versatile pH/temperature multi-responsive copolymer in aqueous environment; 30th edition of PolyChar World Forum on Advanced Materials (PolyChar'30), 11–13 September **2024**, Iasi, Romania.
- 4. **E.-D. Lotos**, M. Karayianni, M. Mihai, S. Pispas; Natural—synthetic hybrid nanostructures by interaction of chitosan with carboxylate ended PNIPAM; 30th edition of the International Conference Progress in Organic and Macromolecular Compounds Conference (MACROIasi 2025), 23-26 September **2025**, Iasi, Romania.
- 5. M. Karayianni, **E.-D. Lotos**, M. Mihai, S. Pispas; Chitosan-*g*-Poly(*N*-isopropylacrylamide) based polyplexes: Effect of DNA length; *30th edition of the International Conference Progress in Organic and Macromolecular Compounds Conference (MACROIasi 2025*), 23-26 September **2025**, Iasi, Romania.

Oral presentations at national and international scientific events (results not included in the thesis):

- 1. F. Bucatariu, M.-M. Zaharia, **E.-D. Lotos**, M.-M. Bazarghideanu, M. Mihai, S. Pispas; Interpolyelectrolyte complexes based on Chit-g-PNIPAM and HSA with pH/temperature responsiveness; 30th edition of PolyChar World Forum on Advanced Materials (PolyChar'30), 11–13 September **2024**, Iasi, Romania.
- 2. M.-M. Zaharia, **E.-D. Lotos**, F. Bucatariu, M.-M. Bazarghideanu, S. Pispas, M. Mihai; *In-situ* synthesis of gold nanoparticles mediated by chitosan-*g*-poly(*N*-isopropylacrylamide); *National Conference of Chemistry XXXVII Edition* (CNCHIM 2024), 25–27 September **2024**, Targoviste, Romania.
- 3. M.-M. Zaharia, E.-D. Lotos, F. Bucatariu, M.-M. Bazarghideanu, D. Rusu, S. Pispas, M. Mihai; Hybrid nanostructures designed by *in-situ* gold nanoparticles synthesis using Chitosan-g-Poly(*N*-isopropylacrylamide); 7th International Conference on Emerging Technologies in Materials Engineering (EmergeMAT), 30–31 October 2024, Bucharest, Romania.

Poster presentations at national and international scientific events (results not included in the thesis):

1. C.-G. Marandiş, M.-M. Zaharia, **E.-D. Lotos**, S. Pispas, I. Mangalagiu, M. Mihai; Composite materials based on thermoresponsive Chitosan-*graft*-Poly(*N*-isopropylacrylamide) hybrid copolymer; *NATO ASI Summer School*, 28 June–5 July **2024**, Smolenice, Slovak Republic.

Member in the implementation team of national research projects:

- 1. PhD student (period 01.03.2022 31.12.2023) within the project *Porous zwitterionic microparticles containing zein and betaine units, with antimicrobial activity and drug delivery capacity*, project code PN–III–P4–ID–PCE–2020–1541, acronym ZwitterZein.
- 2. PhD student (period 01.07.2023 present) in the project *Polysaccharide based* (bio)hybrid nanostructures, project code PNRR–III–C9–2022–I8, acronym HYBSAC.
- 3. PhD student (period 16.07.2025 present) in the project *Multifunctional hybrid* nanostructures formed from natural macromolecules and metals, project code PN–IV–P1–PCE–2023–0738, acronym MacroMet.

Research and professional development stages:

- 1. Short research stage "Porous polymeric materials for medical and environmental applications", 9 May 8 June 2022, Sofia, Bulgaria, participation funded by the project Porous zwitterionic microparticles containing zein and betaine units, with antimicrobial activity and drug delivery capacity (ZwitterZein), project code PN–III–P4–ID–PCE–2020–1541.
- 2. IdEx project "Development of zein-based bioresins", 1 November 2023 31 January 2024, Nice, France, participation funded by the University of Côte d'Azur, project code ANR-15-IDEX-01.
- 3. NATO ASI Summer School Nanomaterials and Nanoarchitectures II. Composite Materials & Their Applications, 28 June 5 July 2024, Smolenice, Slovakia, participation funded by the project *Polysaccharide based (bio)hybrid nanostructures (HYBSAC)*, project code PNRR-III-C9-2022 I8.